REPORT DOCUMENTATION PAGE

Form Approved OMB No. 0704-0188

1. AGENCY USE ONLY (Leave blank)	2. REPORT DATE	3. REPORT TYPE AND DATES COVERED
	1997	Final Report

4. TITLE AND SUBTITLE

Study Of Fast Dynamics Of Photorefractive Crystals

5. FUNDING NUMBERS

F6170896W0267

6. AUTHOR(S)

Dr. Serguey Odoulov

7. PERFORMING ORGANIZATION NAME(S) AND ADDRESS(ES)

Dynamic Holography Group, Institute of Physics
National Academy of Sciences
Science Ave 46,
Kiev 252 650
Ukraine

8. PERFORMING ORGANIZATION REPORT NUMBER

N/A

9. SPONSORING/MONITORING AGENCY NAME(S) AND ADDRESS(ES)

EOARD
PSC 802 BOX 14
FPO 09499-0200

10. SPONSORING/MONITORING AGENCY REPORT NUMBER

SPC 96-4058

11. SUPPLEMENTARY NOTES

12a. DISTRIBUTION/AVAILABILITY STATEMENT

Approved for public release; distribution is unlimited.

12b. DISTRIBUTION CODE

A

13. ABSTRACT (Maximum 200 words)

This report results from a contract tasking Dynamic Holography Group, Institute of Physics National Academy of Sciences as follows: The contractor will perform a service consisting of the study of fast dynamics of photo-refractive recording as described in his proposal. The contractor will examine adjusting frequency detuning of photo-refractive crystals by usin ctro-optic modulation.

14. SUBJECT TERMS

Electronic Devices

15. NUMBER OF PAGES

61

16. PRICE CODE

N/A

17. SECURITY CLASSIFICATION OF REPORT	18. SECURITY CLASSIFICATION OF THIS PAGE	19. SECURITY CLASSIFICATION OF ABSTRACT	20. LIMITATION OF ABSTRACT
UNCLASSIFIED	UNCLASSIFIED	UNCLASSIFIED	UL

AQ

EOARD

Special Project SPC-96-4058

Contract F61708-96-W0267

July 1, 1996 - June 30, 1997

Study of Fast Dynamics of Photorefractive Crystals

FINAL REPORT

Principal investigator:

Serguey G. ODOULOV

Participating in research:

Konstantin V. Shcherbin

Alexander N. Shumelyuk

Ivan M. Stoyka

Institute of Physics
National Academy of Sciences
Kiev, UKRAINE

CONTENT

INTRODUCTION

The photorefractive semiconductor crystals like GaAs, CdTe, InP are sensitive in Near InfraRed region of spectrum [1,2]. Therefore these materials are well fitting to the wavelengths of output radiation of many semiconductor lasers and to the optical fibers, which losses and dispersion are minimum just in the Near InfraRed. The second advantage of semiconductor materials is their relatively short response times as compared to the wide bandgap ferroelectric crystals. These are the reasons for careful attention of the researchers to semiconductor photorefractives.

Cadmium Telluride crystal possesses the best electrooptic quality (largest $n^3 r_{eff}$ value within this group of noncentrosymmetric semiconductors) [3,4]. The crystals CdTe:Ge which we use ensure the largest gain factors known at present without applied electric field [5] and largest specific gain factor (i.e., gain factor per given voltage) for the case of the applied electric field [6]. The study of fast dynamics of photorefractive recording in these crystals is therefore well justified.

Our previous insestigation of photorefractive grating relaxation in GaAs and CdTe [6] pointed out the disagreement of experimentally measured gain spectra with the predicted within the simple one-center model Lorentzian shapes. One of the aims of present study was to find out the possible reasons of this behaviour.

To answer this question we continued the experimental measurement with better equipment purchased within present EOARD Project (New Focus model 4004M electrroptic modulator). We developed also the theory describing the dynamics of photorefractive recording in crystals with two movable

species of charge carriers and compared the experimental results with the predictions of this theory.

The use of new frequency shifting technique (electrooptic modulator) allowed for detailed analysis of the shape of gain spectra in the vicinity of zeroth frequency detuning. As a result it became possible to compare the data obtained by direct measurements of the grating decay with data extracted from gain spectra.

The most important issue of this experiments is the conclusion that for small grating contrast experiments the unusual (deviating from Lorentzian) gain spectrum profile is related to the particular type of charge transport in CdTe:Ge and not to the measurement technique. The second unexpected result is the clear evidence of bipolar conductivity of CdTe:Ge at $\lambda = 1.06$ μm from the flattening or, sometimes, a deep near zeroth detuning frequency in gain spectra. The comparison with the results of our calculations allows for evaluation of the characteristic relaxation rates for transport processes of carriers of different sign.

As usual, some open questions remain with no definite answer when this project is terminated. The complete set of the collected data on intensity dependences of gain factor, of characteristic lifetimes and of crystal conductivity certainly does not fit to simple models with one trap level for each kind of movable carriers. The introduction of the secondary center with its particular population density (induced by laser radiation) and its own characteristic time permits to give a logic explanation to the observed asymmetry of write-readout cycles and to deviation of the measured gain spectra from Lorenzian profile.

At the same time the large amount of collected data on grating relaxation in CdTe:Ge permits to predict the characteristic times for any possible experimental conditions.

1. Experimental procedure.

1.1. Experimental set-up.

A schematic of the experimental set-up is shown in Fig.1. A single-mode single-frequency diod-pumped Nd^{3+}:YAG laser with $\lambda = 1.06$ μm and ≈ 500 mW output power was used in the experiments. The output radiation was polarized in the plane of drawing. The attenuator Att allowed for decreasing of the laser power to 0.5 mW. A part of intensity separated by the beamsplitter BS1 was used to monitor permanently the laser output power. The beamsplitter BS2 devided the laser beam into two with the intensity ratio roughly equal 1:2. The strongest of two beams was sent to polarisation beamsplitter PBS. With the $\lambda/2$-phase retarder placed in front of PBS it was possible to control the intensity ratio of two beams I1:I2 splitted from PBS. The beam with the vertical polarization was sent to the electrooptic modulator (EOM1); with the applied voltage the EOM1 changed the optical path keeping the same polarization. Transmitted through EOM1 beam was sent to the second $\lambda/2$-phase retarder to turn its polarization to 90°. The polarizer P was used to clean-up the resulting polarization to be exactly horizontal. Two horizontally polarized waves with the intensities I1 and I2 impinged upon the sample at an angle 2θ and wrote a grating with the grating spacing $\Lambda = (\lambda/2\sin\theta)$. All samples were cut in such a way that their

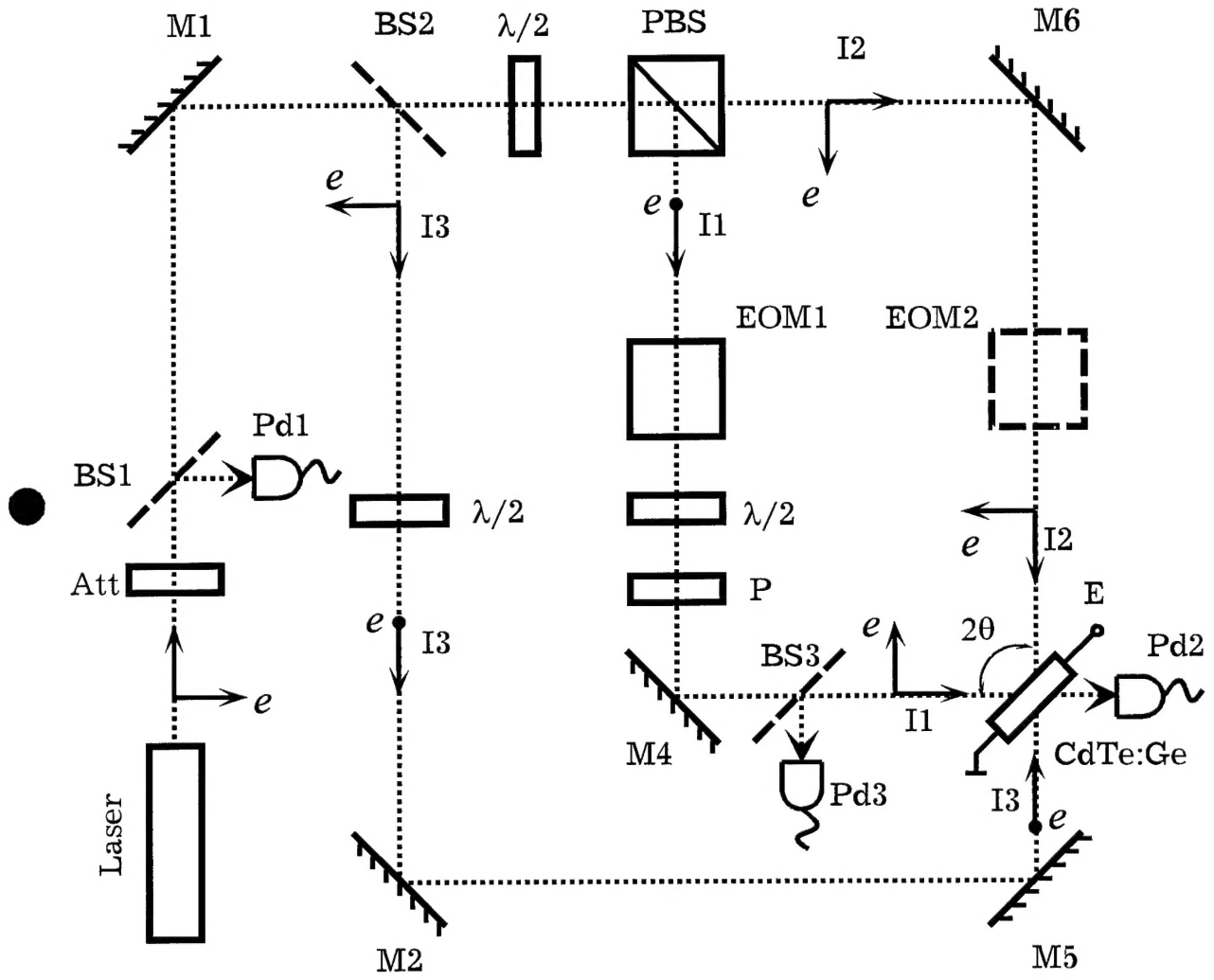
M1
BS2
λ/2
PBS
I2
M6
e
I3
e
I1
e
EOM1
EOM2
Pd1
BS1
λ/2
λ/2
e
I2
Att
P
E
e
I3
e
2θ
BS3
Pd2
e
I1
M4
CdTe:Ge
Pd3
I3
e
Laser
M2
M5

Fig. 1.

side faces were normal to [111] direction. This allowed for the optimized recording of the transmission grating with grating vector K || [111] [7,8]. To apply to the sample the external field the silver past electrodes were deposited to the side faces.

The grating recording was performed either by the beams with Gaussian transverse distribution of intensity or with the expanded beams (less than 10% intensity variation over whole sample cross section). The beam expanders were placed just in front of the sample. The power of the wave I1 transmitted through the crystal was monitored by the detector PD1. In the path of the second light beam one extra electrooptic modulator (EOM2) was placed to switch if necessary the transmitted beam polarization to 90°.

The third beam from BS2 was directed by mirrors M2 and M5 to the sample from the opposite side to counterpropagate with respect to the beam I2. To avoid the recording of the reflection gratings in the sample the polarization of the readout wave was rotated to 90° with the help of one more $\lambda/2$-phase retarder. A part of light of the beam I3 was diffracted from the recorded grating in the direction of the beam I1. To evaluate the intensity of the diffracted wave the semitransparent mirror BS3 was used, which was reflecting the diffracted beam to the detector PD3.

All stages of the experiment including the data ascuisition and processing were controlled by a computer. The electric outputs of the detectors were digitalized with AD Converter. To study the temporal variations of the light beam intensity the numerical oscilloscope was used. The driving signals for electrooptic modulators were produced by the signal generator (Stanford Research Systems Synthesized Function Generator model

DS345) and amplified by high voltage Trek Amplifier (model 609C-6). The tailoring of the pulse shape and the control of pulse amplitude and frequency was done with the personal computer. The same computer was collecting data from AD Converter Card and from numeric oscilloscope.

The described set-up allowed for the detailed measurements of the spectral dependences of the beam coupling and of the diffraction efficiency. To shift the frequency of one beam the ramp voltage was applied to the electrooptic modulator EOM1, with the peak-to-peak amplitude providing the 2π-change of the phase of the transmitted wave. In such a manner the frequency detuning $\Delta\omega = 2\pi f$ (in radians per second) was introduced in beam I1, with f being the frequency of saw-tooth signal in Hz.

To study the two-beam coupling the standard gain factor $\Gamma = (1/d) \ln(I_s/I_{so})$ was measured, where I_s and I_{so} are the intensities of the transmitted signal beam with and without the pump wave switched on, respectively, d is the crystal thickness. To study the spectra of the diffraction efficiency η the intensity of the diffracted wave was measured by the detector PD3 as a function of the frequency detuning $\Delta\omega$.

In independent experiments the temporal variations of the space charge build-up and decay were measured. Two techniques were used to destroy the grating while keeping the total intensity of light nearly constant: In first technique the signal shown in Fig.2 was sent to the electrooptic modulator EOM1. This signal is in fact the regular sequence of rectangular pulses filled with the high-frequency (20 KHz) sinusoidal oscillations. This frequency to our knowledge is much higher than the reciprocal relaxation

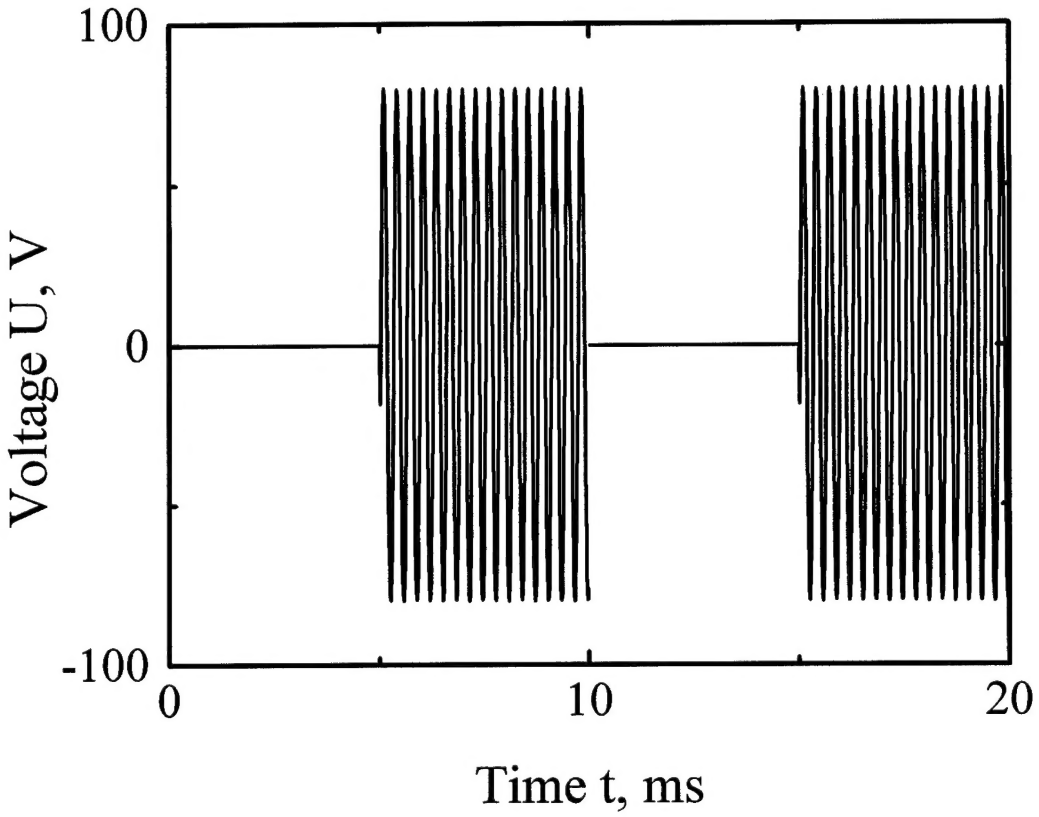

Fig. 2.

time of the sample $2\pi f >> 1/\tau$ for the intensities of the recording beams and spatial frequencies of the recorded gratings used in our experiments.

At initial part of every period (see Fig.2), with no voltage sent to the EOM1, the grating is developing until the steady state is reached. With the onset of sinusoidal oscillations (Fig.2) the recording fringes start to vibrate. With the specially chosen amplitude of vibrations the grating appears to be washed out to identical zero efficiency. Note that the averaged intensity of light remains exactly the same as without fringe motion. Therefore the measurements of the dynamics of grating build-up and decay occurs exactly at the same conditions as the measurements of the gain spectra and spectra of the diffraction efficiency.

The amplitude of vibrations needed to erase completely the grating was found in following way. If the phase φ of the beam I1 is modulated with the help of electrooptic modulator EOM1

$$\varphi(t) = \varphi_o \sin(\Delta\omega t), \qquad (1)$$

the fringe visibility is changing as [9]:

$$m = m_0 \sum J_n(\varphi_0) \exp(in\Delta\omega t) \qquad (2)$$

and the space charge field is modulated as

$$E_{sc}(t) \sim -im_0 E_D \sum \left[J_n(\varphi_0) \exp(in\Delta\omega t)/(1 + in\Delta\omega t) \right], \qquad (3)$$

where $J_n(\varphi_0)$ is the Bessel function of n-th order.

As the diffraction efficiency of the grating η is proportional to the square of the refractive index change Δn (which in turn is linear in E_{sc}) we finally get for static (stationary) grating

$$\eta \sim J_0^2(\varphi_0). \qquad (4)$$

Note that for the crystal with the characteristic relaxation time τ all higher temporal harmonics of the space charge field will be negligibly small if $\tau >> 1/\Delta\omega$.

To determine the first zero of Bessel function which ensures complete inhibition of grating efficiency we measure the dependence of $\eta = \eta(U)$, where U is the voltage on electrooptic modulator.

The frequency of voltage modulation as it was already mentioned was 20 KHz. No intensity modulation of the diffracted wave was observed for this frequency. First, this proves that the restriction $\tau >> 1/\Delta\omega$ is satisfied, second, this allows for easy measurement of the mean value of η.

Voltage dependence of the diffraction efficiency is shown in Fig.3. The solid line gives the best fit to the squared Bessel function (Eq.4). The diffraction efficiency vanishes at U = 80 V. We use in what follows this amplitude of frequency modulated voltage (20 KHz) on EOM1 (see Fig.2) to destroy the grating.

The second technique of grating switch-on/switch-off consists of rapid switch of the polarization of one of two recording waves to orthogonal one. To do it an extra electrooptic modulator EOM2 is placed between the mirror M3 and the crystal, which turns the polarization of this beam to 90°. With the external field applied two waves becomes orthogonally mutually polarized, the contrast of the recording fringes decreases to zero and the grating vanishes. In this technique a slight variation of the total intensity occurs because of different Fresnel reflections from input/output faces for two

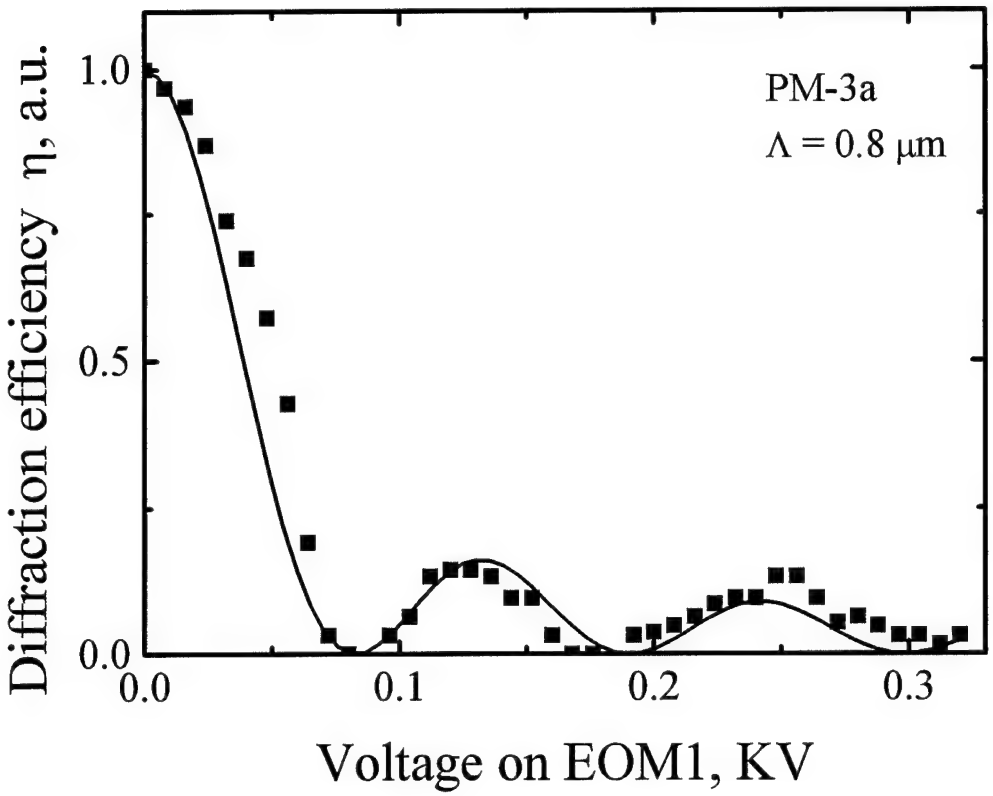
Diffraction efficiency η, a.u.
1.0
0.5
0.0
0.0
0.1
0.2
0.3
PM-3a
Λ = 0.8 μm
Voltage on EOM1, KV

Fig. 3.

orthogonally polarized waves. In addition, with the identical (vertical) polarization of two counterpropagating waves (2 and 3) the reflection grating recording starts to be possible. In spite of the fact that both factors produce only marginal effect on the grating recorded by waves 1 and 2 we mostly used the previous technique of grating erasure by vibrating fringe pattern.

1.2. Calibration experiments.

Before to start with the measurements we performed a set of calibration experiments. At first the variable polarization beam-splitter (including $\lambda/2$-phase retarder and PBS) was calibrated. The intensities of the beams 1 and 2 were measured as a function of the tilt angle β of $\lambda/2$-phase retarder (see Fig.4a). The intensity of the third beam I3 which is not affected by the rotation of $\lambda/2$ phase retarder is also shown in Fig.4a for reference.

When working with unexpanded laser beams an averaged value of the light intensity was calculated taking into account that the illuminated area on the sample input face is changing with the recording angle θ. Note that for our particular set-up the path difference for the beams 1 and 2 is close to zero and therefore the crossections of both beams are exactly the same while the beam 3 usually passes a larger distance before entering sample. When the recording angle is increasing the sample is moved closer to the beamsplitter BS3; consequently the area illuminated by beams 1 and 2 is decreasing and area illuminated by beam 3 in increasing. All these factors were taken into consideration when calculating the mean intensity and effective fringe visibility inside the sample.

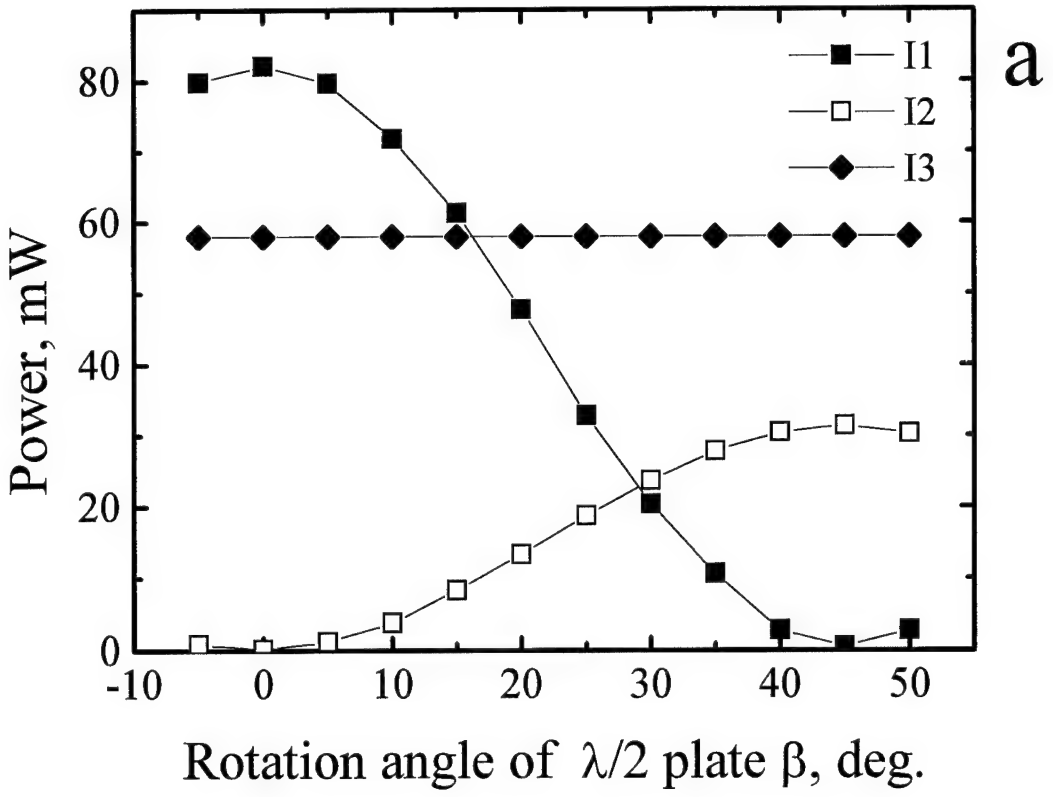
a
I1
I2
I3
Power, mW
0
20
40
60
80
-10
0
10
20
30
40
50
Rotation angle of λ/2 plate β, deg.

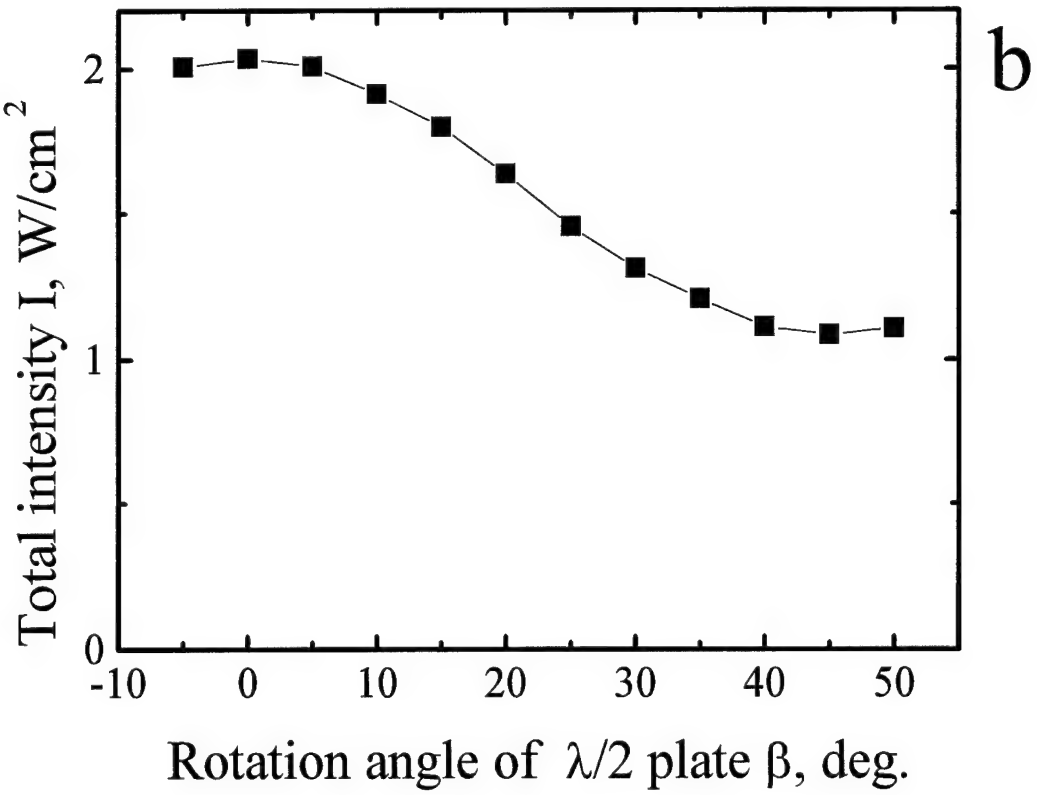
b
Total intensity I, W/cm 2
0
1
2
-10
0
10
20
30
40
50
Rotation angle of λ/2 plate β, deg.

Fig. 4.

In addition, when changing the intensity ratio of the recording waves we affect also the total intensity inside the samle because a part of the signal intensity is reflected by the beamsplitter BS3 used for detection of the diffracted from the grating wave. Figure 4b represents the total intensity of three Gaussian beams as a function of $\lambda/2$ plate rotation angle β for grating spacing 1.2 μm.

Figure 5a represents the dependence of beam intensity ratio I1/I2 on rotation angle β while Figure 5b gives the similar dependence of fringe visibility m. Note that the intensity of all three beams was put in denominator when calculating m:

$$m = \frac{2\sqrt{I1\,I2}}{I1 + I2 + I3}. \qquad (5)$$

The equipment used for frequency shifting in our experiments has an upper limit of high-quality performance. The largest possible frequency shift is limited by the High Voltage Trek Amplifier. To evaluate this upper limit we were measuring the beat frequency mark of the two recording waves using the detector placed behind an aperture smaller than the fringe spacing. An example of beat frequency mark for f = 100 Hz is shown in Figure 6a. When the voltage is running idle we observe an abrupt peak in intensity which is due to the fast change of the voltage on EOM1. This peak can influence the results of measurements at frequencies comparable with the inverse pulse width. Figure 6b shows the intensity variations around peak in larger time scale. Note that peak itself is followed by damped oscillations with as minimum 3 well resolved periods. We chose the third pulsation with the width 100 μs for our estimates: The limiting frequency which corresponds to

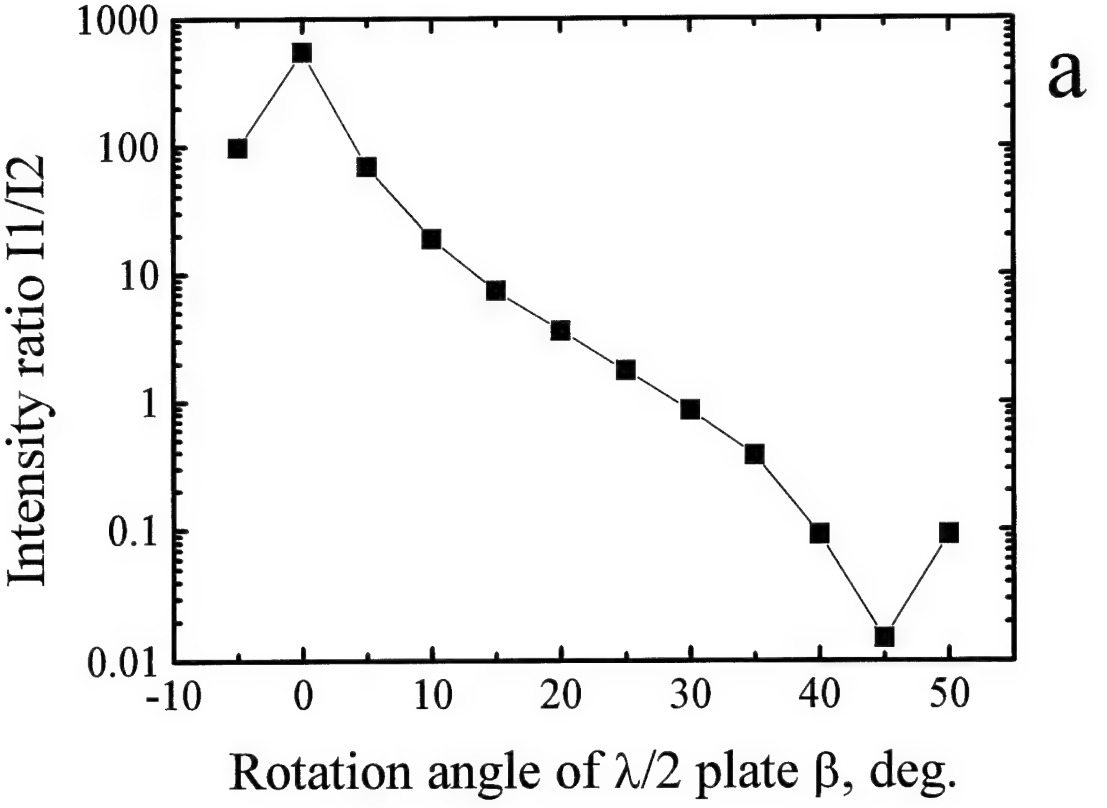
a
1000
100
10
1
0.1
0.01
Intensity ratio I1/I2
-10
0
10
20
30
40
50
Rotation angle of λ/2 plate β, deg.

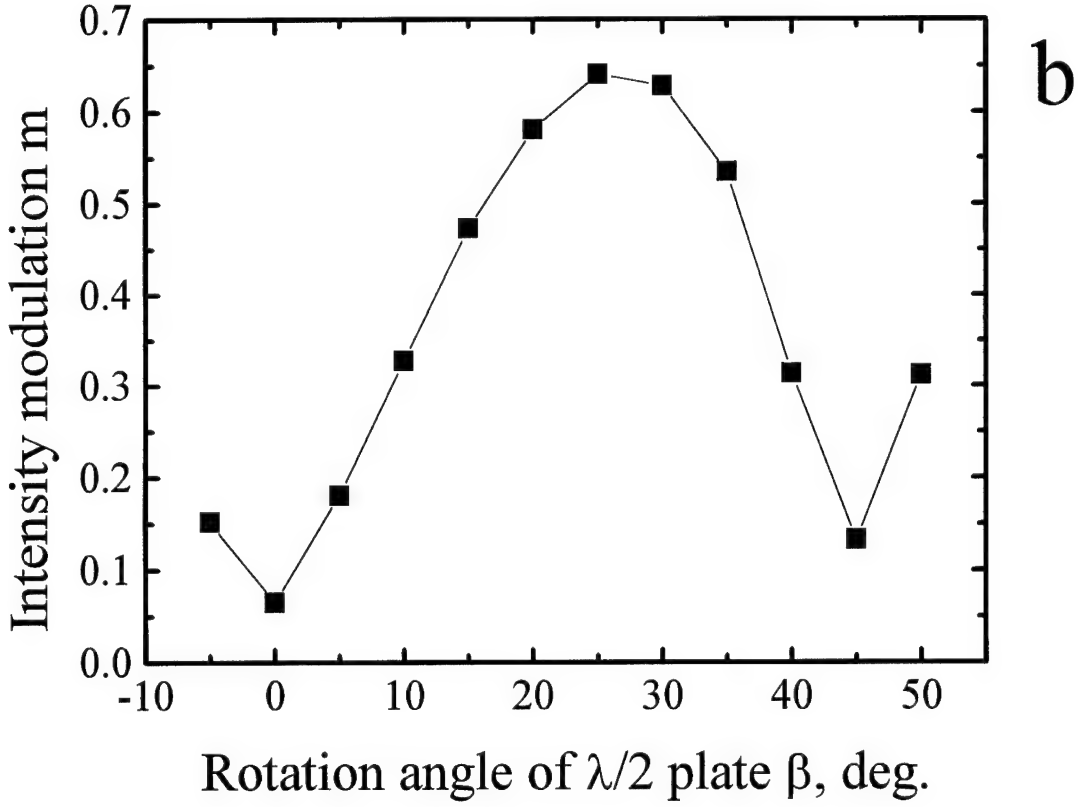
b
0.7
0.6
0.5
0.4
0.3
0.2
0.1
0.0
Intensity modulation m
-10
0
10
20
30
40
50
Rotation angle of λ/2 plate β, deg.

Fig. 5.

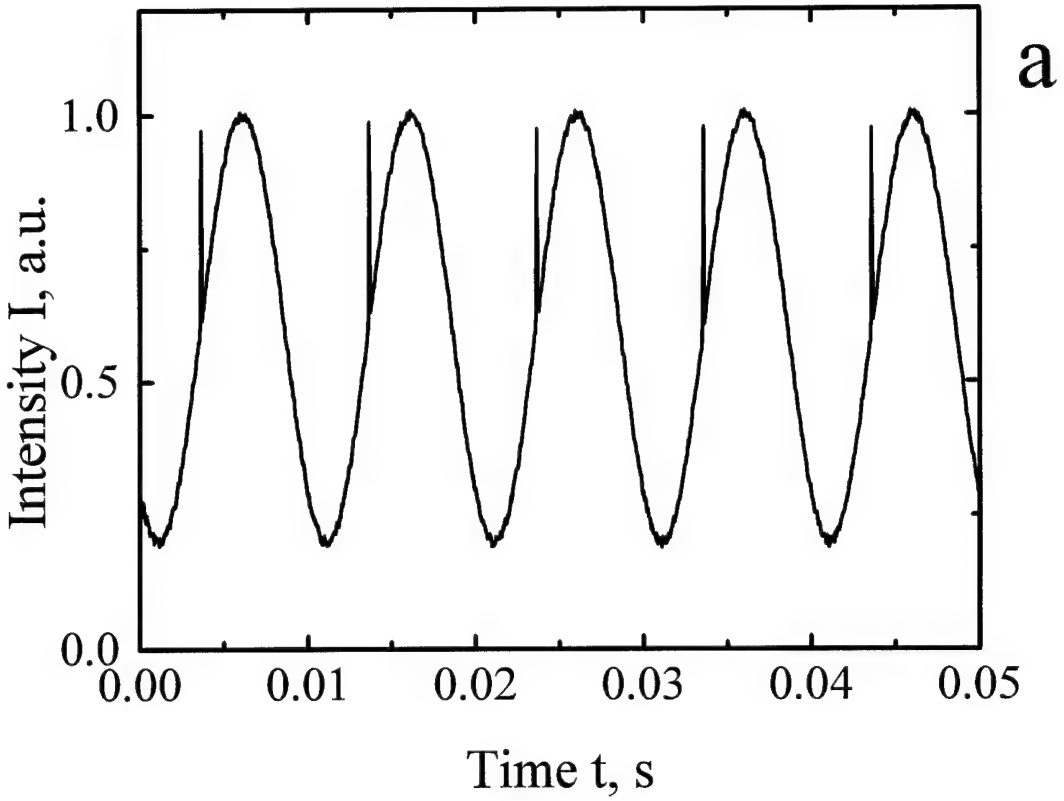
a
1.0
0.5
0.0
Intensity I, a.u.
0.00
0.01
0.02
0.03
0.04
0.05
Time t, s

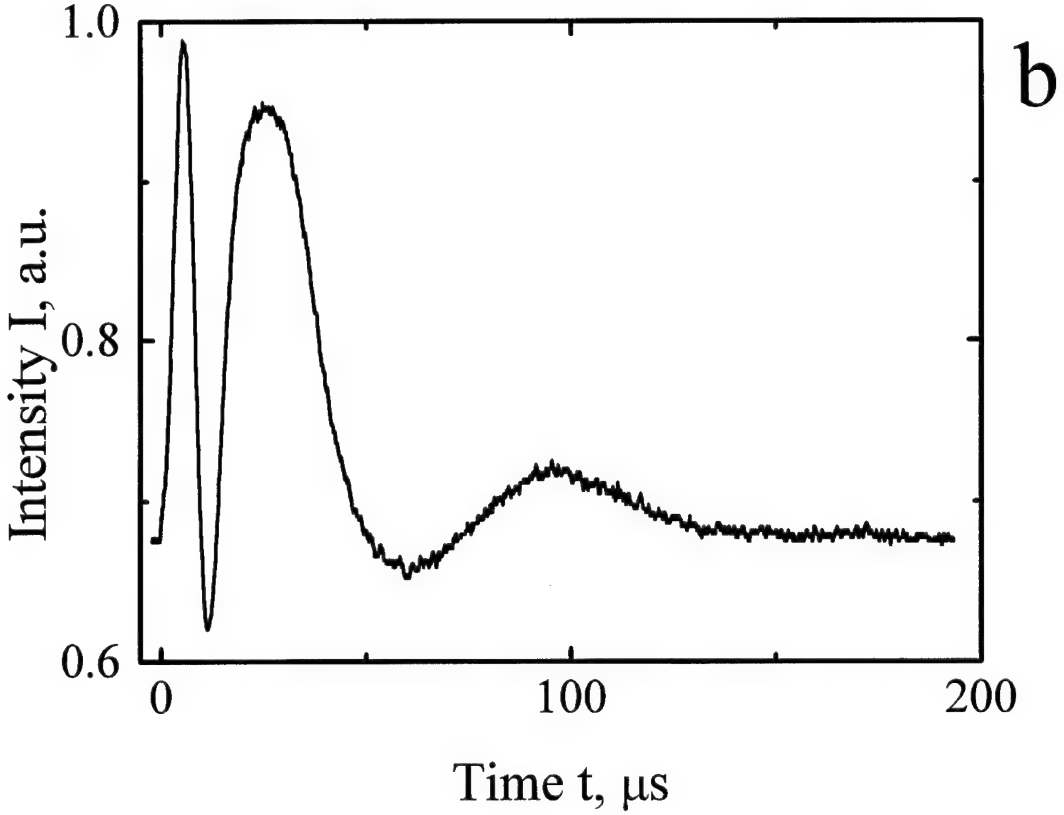
b
1.0
0.8
0.6
Intensity I, a.u.
0
100
200
Time t, μs

Fig. 6.

this pulse width will be 10 KHz. To get the reliable data in our measurements with this electrooptic frequency shifter we limit ourselves by ten times smaller frequency detuning working with $f \leq 1$ KHz.

2. Dynamic properties of diffusion-recorded gratings in CdTe.

With the techniques described above the spectral profiles of the gain factor and of the diffraction efficiency of the grating were measured for various CdTe:Ge samples, for different intensity ratios of the recording beams and different spatial frequencies of the recorded gratings.

2.1. Nearly frequency degenerate wave mixing in CdTe.

One can represent the coupling strength for the grating recording with nearly frequency degenerate light waves in photorerfractive crystal with the single exponential relaxation as [10,11]:

$$\gamma = \gamma_0 /(1 + i\Delta\omega\tau), \qquad (6)$$

where γ_0 is the coupling constant for purely degenerate case, $\Delta\omega = 0$, which may be, in principle, the complex value. This can be rewritten as

$$\gamma = [\gamma_0 /(1 + \Delta\omega^2\tau^2) - i\,[\gamma_0\,\Delta\omega\tau/(1 + i\Delta\omega^2\tau^2)] = \gamma' + i\,\gamma'' , \qquad (7)$$

The first term in the right hand side of this equation, γ', describes the amplitude of the $\pi/2$-shifted component of the grating and therefore gives the spectrum of the gain factor Γ

$$\Gamma = \Gamma_0 /(1 + \Delta\omega^2\tau^2) , \qquad (8)$$

where $\Gamma_0 = 2\gamma_0$ is the gain factor for strict degeneracy.

The second term, γ'', is giving the amplitude of the unshifted part of the grating. Taking into account that the waves diffracted from the shifted and from the unshefted components of a grating are $\pi/2$-out of phase the overall diffraction efficiency will be a sum of two contributions, i.e.,

$$\eta \propto (\gamma')^2 + (\gamma'')^2 = \gamma_0^2 /(1 + \Delta\omega^2\tau^2) . \qquad (9)$$

We can expect therefore the same Lorenzian shape for both diffraction efficiency spectrum and spectrum of gain factor. Note that the widths (HWHM) of both dependences are expected to be the same, too.

2.2. Experimental results.

All crystals used in our experiments were germanium doped but with different aftergrowth thermal treatement. We will use in what follows the notations of the samples given by the producer (Chemical Department of Chernovtcy State University, Ukraine). The crystals of PM-series were cut from the different parts of the same boul. Some properties of the samples are presented in table 1.

Table 1.

Sample	Dopant	Γ_{max} , cm^{-1}	Shape of gain spectrum
PM-1a	Ge	0.53	flat maximum
PM-2	Ge	0.55	small deep at $\Delta\omega = 0$
PM-3a	Ge	0.65	
KT-51-95	Ge, Sb	0.7	
N3	Ge	0.65	pronounced deep at $\Delta\omega = 0$

2.2.1. Spectra of gain factor and diffraction efficiency.

The typical gain spectra and diffraction efficiency spectra for ПМ-3a CdTe crystal at fringe spacing 0.8 and 1.2 μm are shown in Figures 7 and 8, respectively.

We should note right away that in all experiments with CdTe we have never seen a pure Lorenzian profile whatever were the experimental conditions. Possible reason for this deviation could be a more complicated, nonexponential grating decay. To check this possible explanation we are measuring the temporal variation of the grating efficiency during recording and erasure directly.

2.2.2. Dynamics of the grating recording-erasure.

Figure 9a represents the results of the experiments for sample PM-3a at Λ = 1.2 μm and beam intensity ratio 1:1 (fringe visibility with the intensity of counterpropagating beam I3 taken into account, m = 0.63). Figure 9b represents the log plot of the grating decay curve. The similar curves for larger disbalance of the recording wave intensities 1:10 (m = 0.44) are shown in Fig.10. The grating decay is obviously nonexponential.

As the spectra of the gain factor and diffraction efficiency deviate from the Lorenzian profile, the decay of the gratings recording in all CdTe crystals at all experimental conditions (fringe spacings from 0.8 to 3.4 μm, the total intensity from 50 mW/cm^2 to 3 W/cm^2, recording with Gaussian or expanded beams) is not exponential. Note also, that the recording-erasure

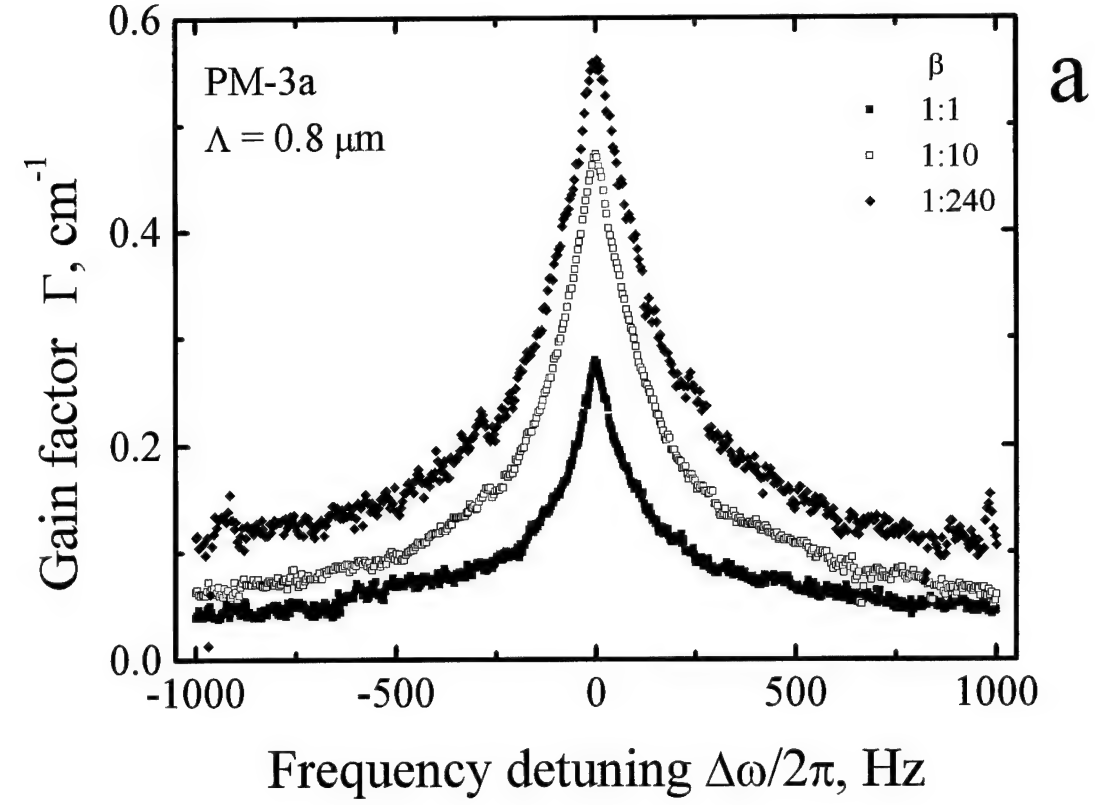
PM-3a
Λ = 0.8 μm
β
1:1
1:10
1:240
Gain factor Γ, cm-1
0.6
0.4
0.2
0.0
-1000
-500
0
500
1000
Frequency detuning Δω/2π, Hz

a

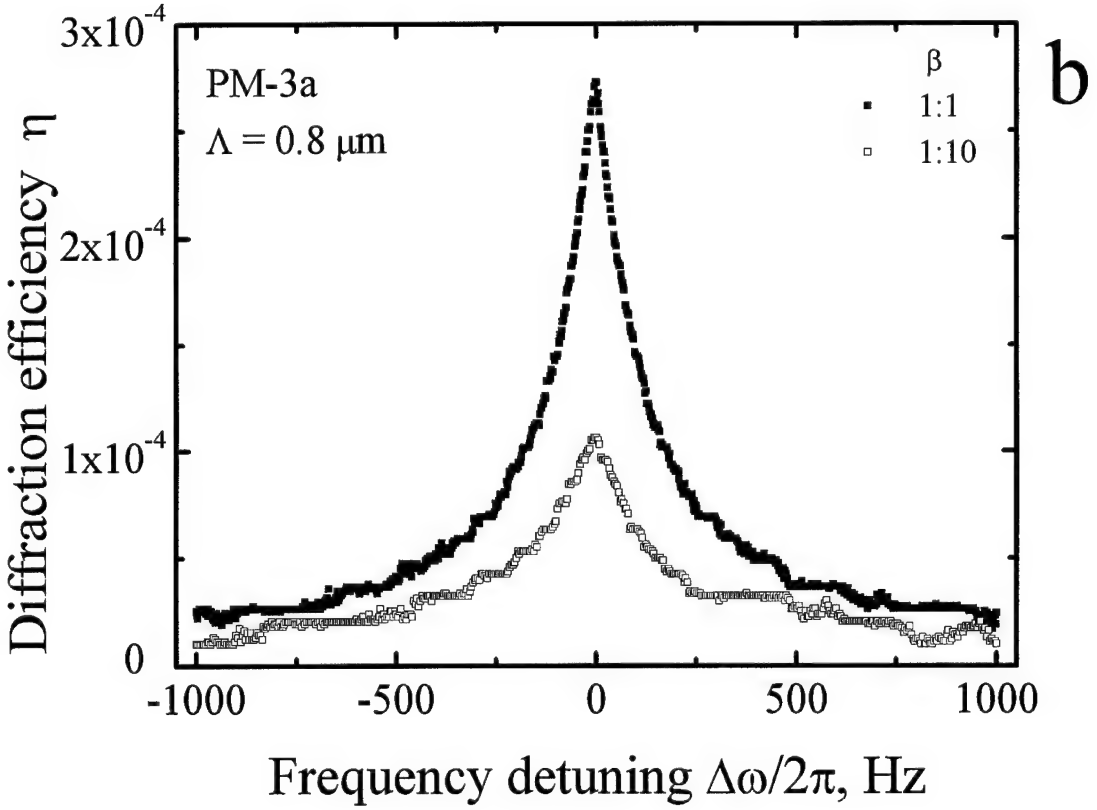
PM-3a
Λ = 0.8 μm
β
1:1
1:10
Diffraction efficiency η
3x10-4
2x10-4
1x10-4
0
-1000
-500
0
500
1000
Frequency detuning Δω/2π, Hz

b

Fig. 7.

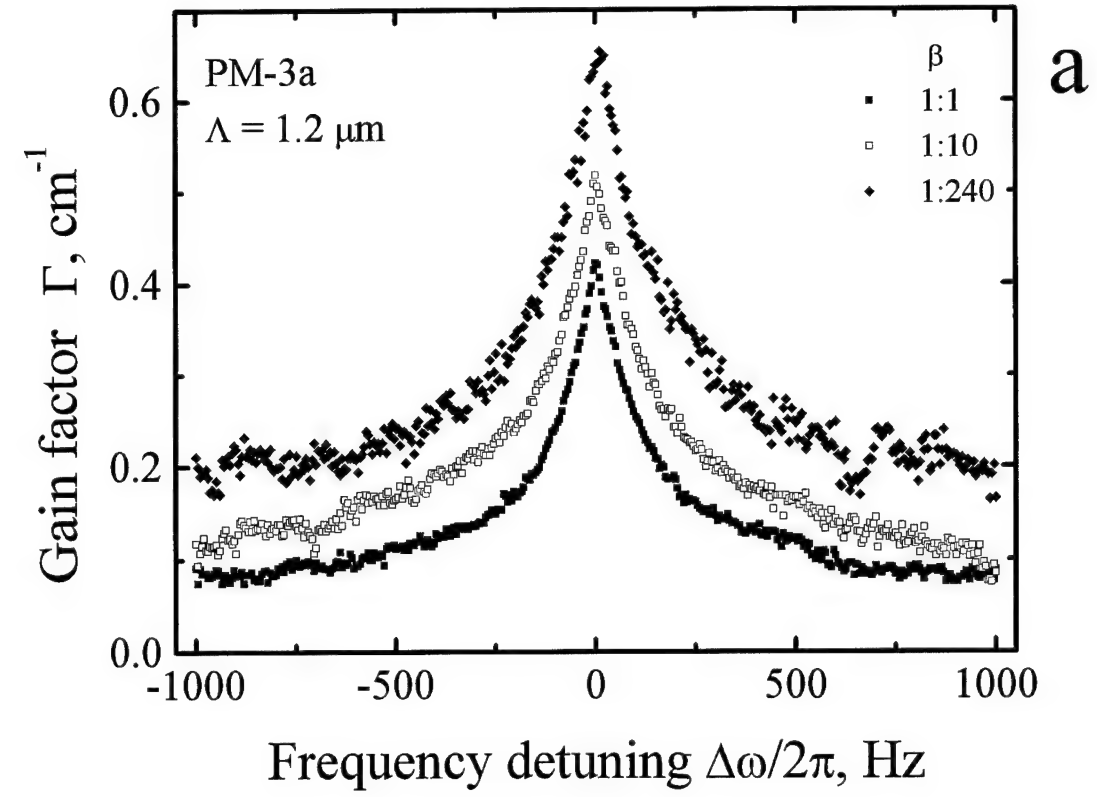
PM-3a
Λ = 1.2 μm
β
1:1
1:10
1:240
a
Gain factor Γ, cm-1
0.0
0.2
0.4
0.6
-1000
-500
0
500
1000
Frequency detuning Δω/2π, Hz

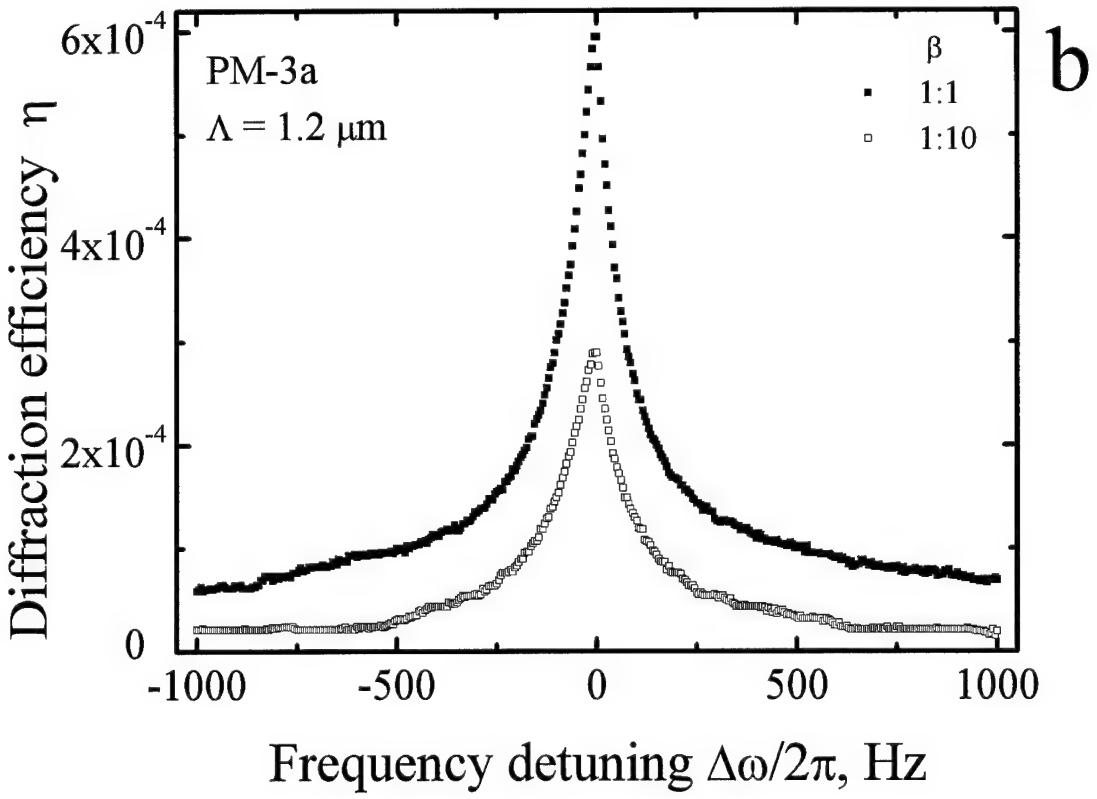
PM-3a
Λ = 1.2 μm
β
1:1
1:10
b
Diffraction efficiency η
0
2x10-4
4x10-4
6x10-4
-1000
-500
0
500
1000
Frequency detuning Δω/2π, Hz

Fig. 8.

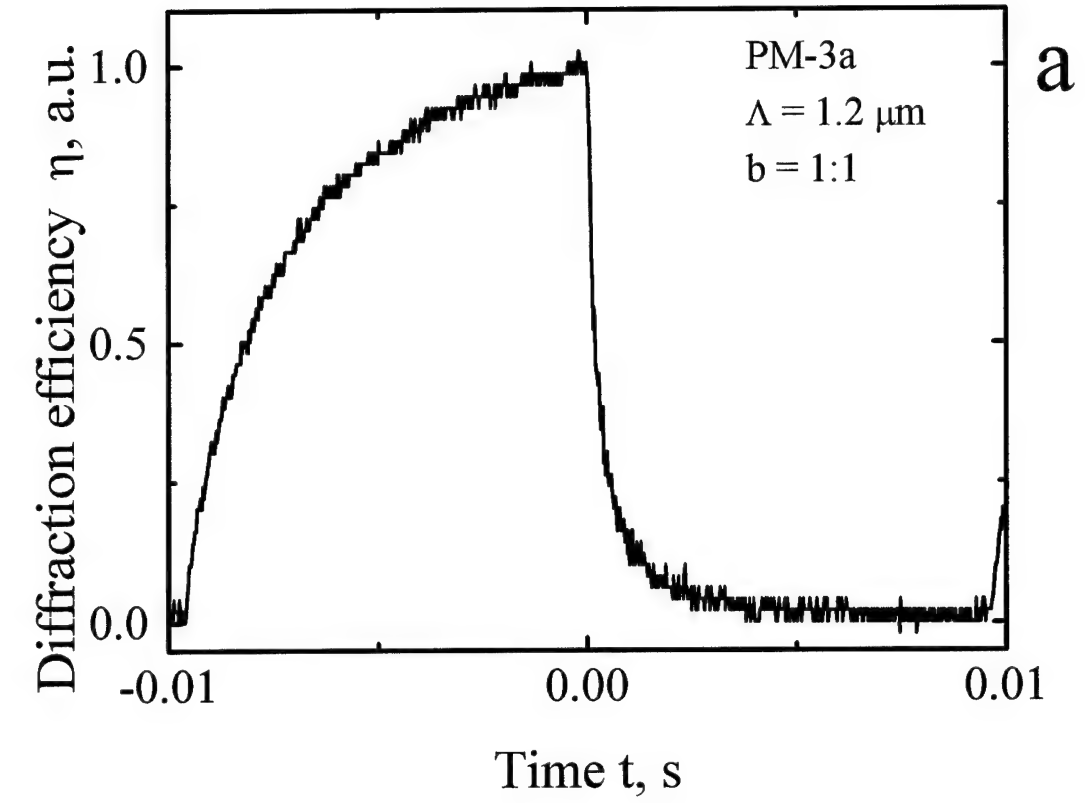
PM-3a
Λ = 1.2 μm
b = 1:1
a
Diffraction efficiency η, a.u.
1.0
0.5
0.0
-0.01
0.00
0.01
Time t, s

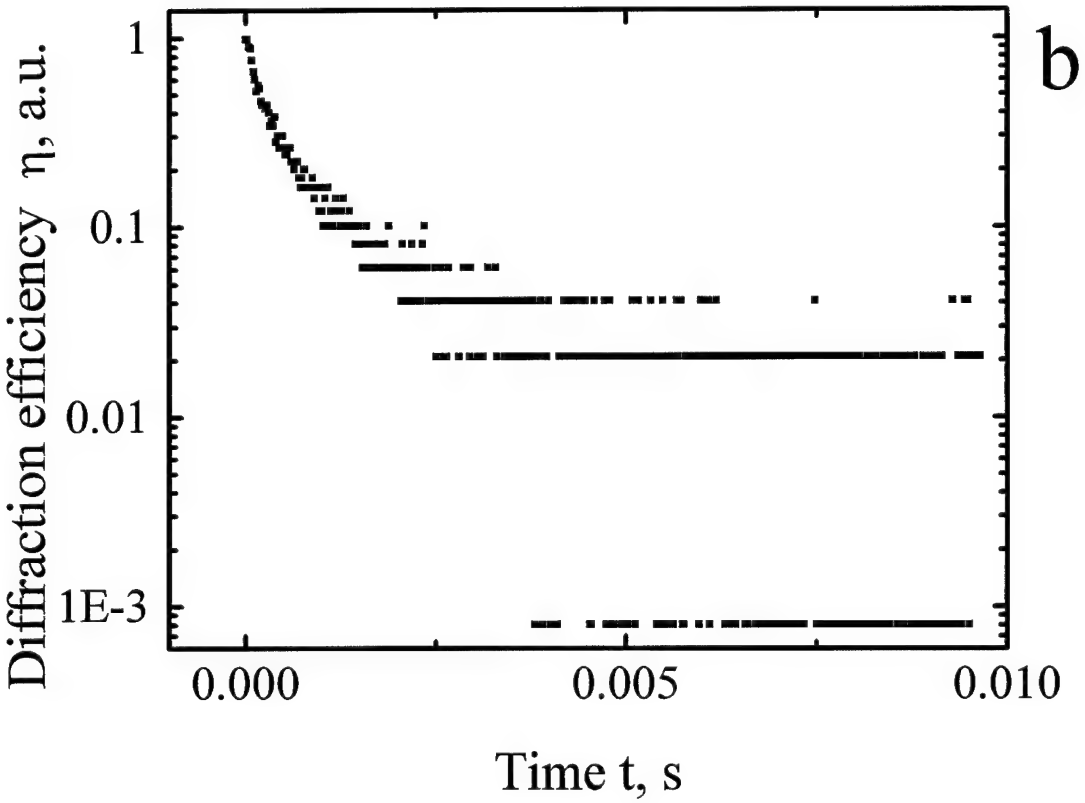
b
Diffraction efficiency η, a.u.
1
0.1
0.01
1E-3
0.000
0.005
0.010
Time t, s

Fig. 9.

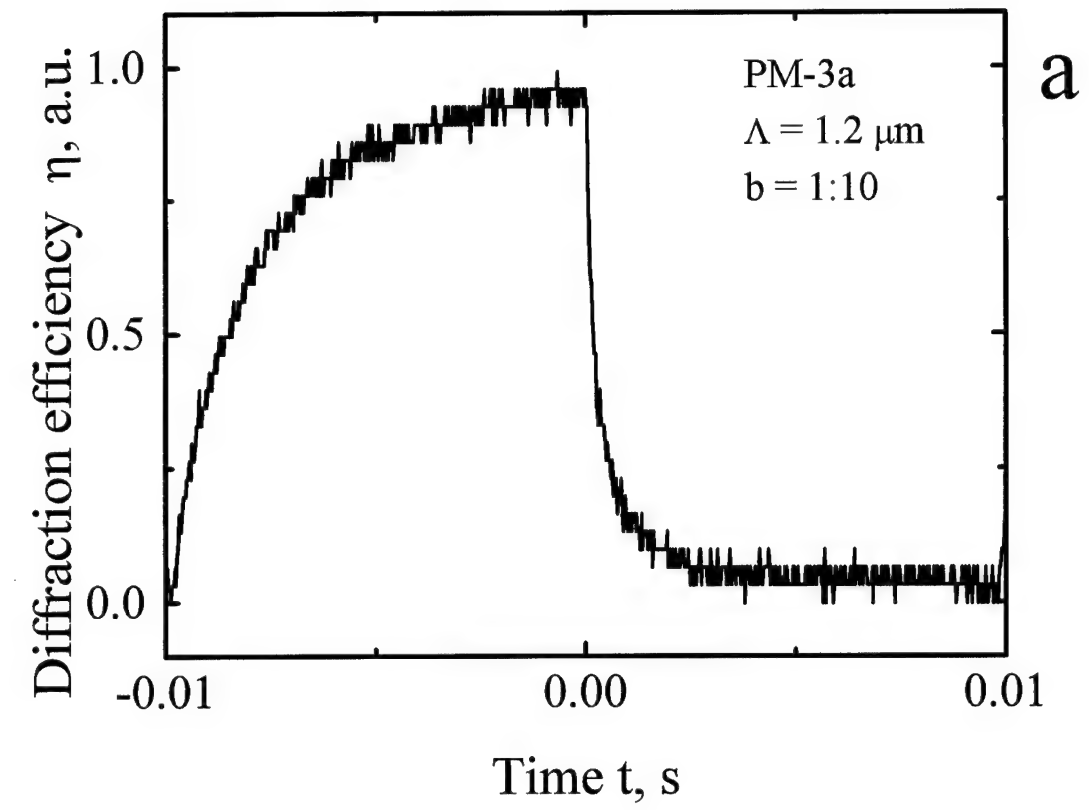
a
PM-3a
Λ = 1.2 μm
b = 1:10
Diffraction efficiency η, a.u.
1.0
0.5
0.0
-0.01
0.00
0.01
Time t, s

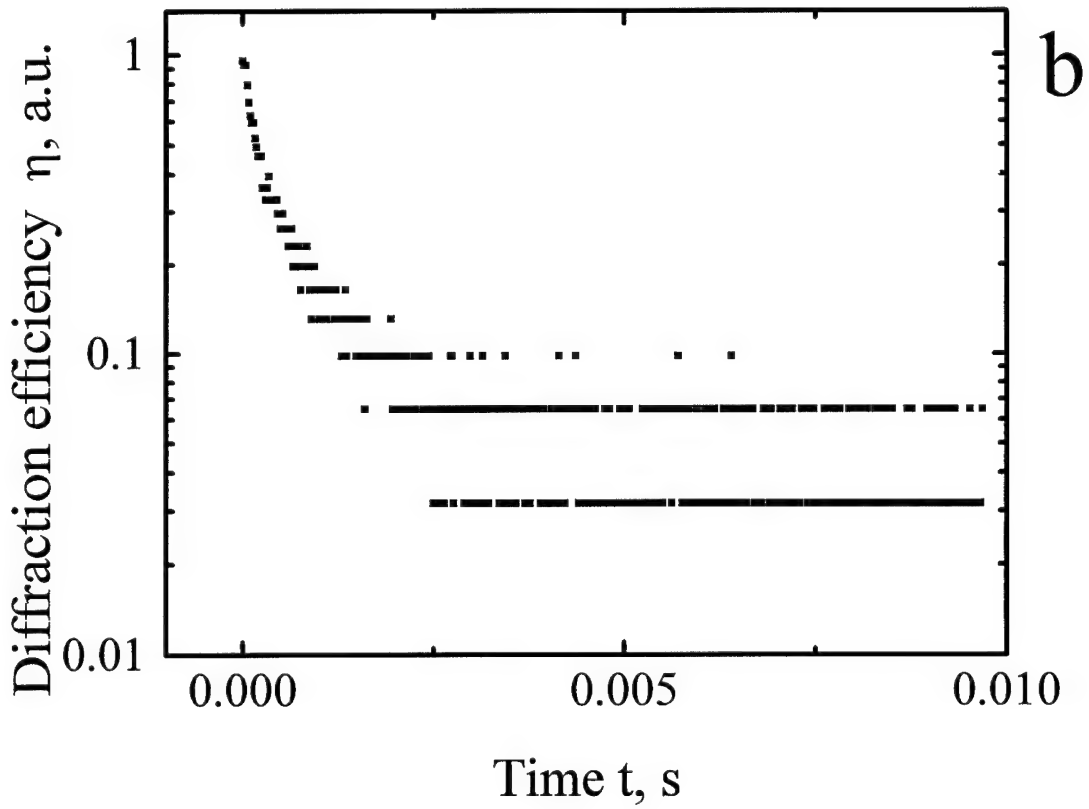
b
Diffraction efficiency η, a.u.
1
0.1
0.01
0.000
0.005
0.010
Time t, s

Fig. 10.

cycle is asymmetric: The grating recording appears to be much slower than the grating decay.

Figure 11a shows the dynamics of the grating recording-erasure, registered with the polarization technique of grating erasure (change of polarization of the beam I2 with EOM2). The data are recorded with PM-3a sample and fringe spacing 1.2 μm, for beam intensity ratio 1:1. Figure 11b gives the decay of the diffracted beam intensity during optical erasure. Once more time we get the decay curve deviating from single exponent. The similarity of the results for two different techniques of grating optical erasure proves that the results are not affected by the measurement procedure but are related to physical processes which are not taken into account in simple model discussed in the beginning of this chapter. It is quite clear that with substantially nonexponential decay curves we can not expect purely Lorenzian spectrum profiles for the gain factor and for diffraction efficiency.

2.3. Discussion. Possible factors affecting the frequency detuning spectra.

It is known [12] that the temporal behavior and the spectrum are interrelated by the Fourier transform

$$\Delta n(\Delta\omega) \propto \boldsymbol{F}\{\Delta n(t)\}. \qquad (10)$$

We check this relationship by comparing the directly measured spectrum and spectrum obtained from the Fourier transform of the grating decay, measured at the same conditions. Figure 12a shows the decay curve for a grating recorded in PM-3a sample by beams with 1:1 intensity ratio at Λ = 1.2 μm. The amplitude of complex $\Delta n(\Delta\omega)$ calculated as Fast Fourier

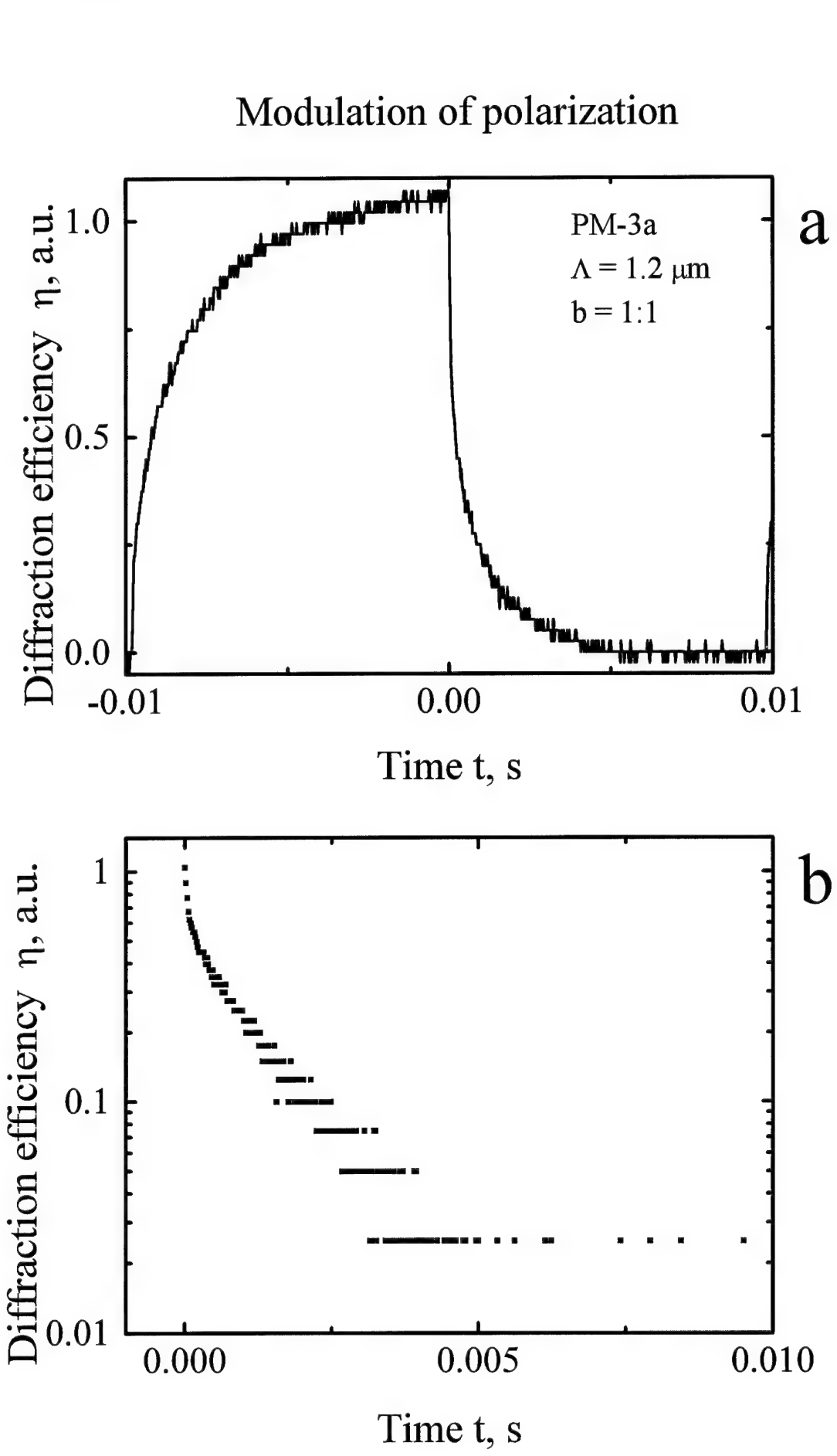
Modulation of polarization
Diffraction efficiency η, a.u.
1.0
0.5
0.0
-0.01
0.00
0.01
Time t, s
PM-3a
Λ = 1.2 μm
b = 1:1
a
Diffraction efficiency η, a.u.
1
0.1
0.01
0.000
0.005
0.010
Time t, s
b

Fig. 11.

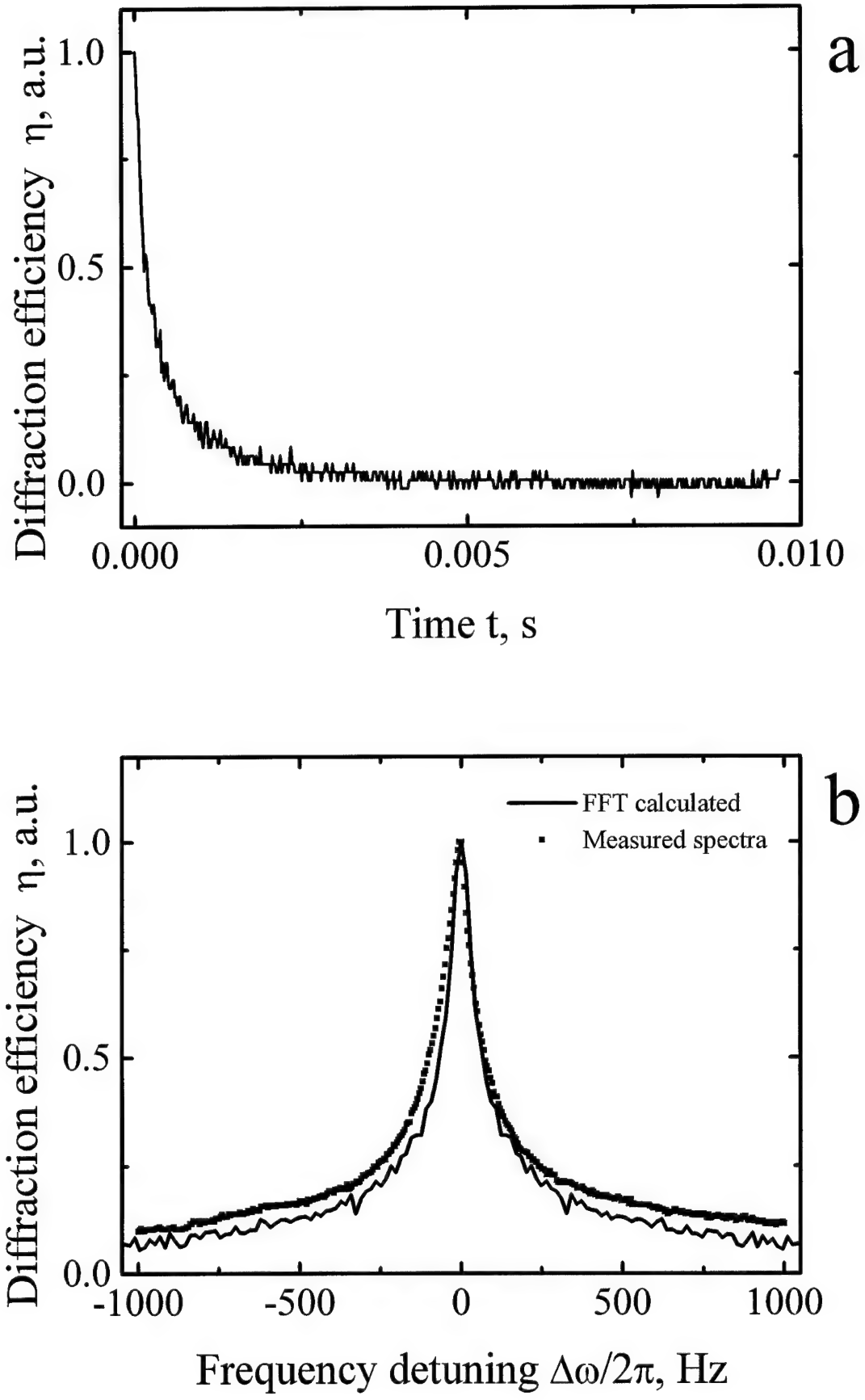
a
Diffraction efficiency η, a.u.
1.0
0.5
0.0
0.000
0.005
0.010
Time t, s
b
FFT calculated
Measured spectra
Diffraction efficiency η, a.u.
1.0
0.5
0.0
-1000
-500
0
500
1000
Frequency detuning Δω/2π, Hz

Fig. 12.

Transform (FFT) from this curve is shown in Fig.12b by solid line while the experimentally measured spectrum of the diffraction efficiency is shown by small squares. A good agreement of both curves is evident. We conclude from this comparison that the reason of deviation of the decay curves from single exponent is the same as the reason of deviation of spectra from Lorenz shape. We believe this reason is related to oversimplified model of charge transport which we adopted in this study.

In one of the following Sections we will show unambiguously that electron-hole competition is the other reason of the strong deviation of the measured spectra from Lorenz profiles.

Let us analyze the possible reasons of the unusual shape of measured spectral profiles.

2.3.1. Nonuniform intensity distribution because of absorption.

It is well known that the dielectric relaxation time in the illuminated crystal is a function of the light intensity. In the absorbing material the total intensity of the recording waves is diminishing with the crystal depth, therefore the characteristic relaxation time of a grating also becomes a function of the propagation coordinate. In other words, for different layers of the sample (with different intensity of the recording waves) we will get different spectra; the integral spectrum therefore will have a profile deviating from Lorenzian.

Our previous attempts to describe this effect analytically [6] were not successful: in spite of the fact that we got a very nice fit to the measured

spectral profile the fitting parameter (which is a linear absorption constant) was far away from the directly measured value.

Our new data also can not be fitted to this model with measured absorption constant of the order of 1 cm^{-1} . In all our experiments the counterpropagating light beam was sent to the sample to read out the recorded grating. The intensity of this auxiliary beam was comparable with the intensity of forward going beams. Thus the nonuniform intensity distribution was corrected to a certain extent: The dependece of the overall intensity on propagation coordinate becomes less strong as compared with only two copropagating recording beams. The deviation from the Lorenz profile is still visible also in three beam experiments. Thus we believe that the observed discrepancy can not be attributed to the effect of linear absorption.

It should be mentioned however that for the samples with stronger absorption (then $\alpha \approx 1$ cm^{-1} for our samples) the intensity variations with the sample depth will immediately result in nonexponential decay and non Lorenzian profiles.

2.3.2. Spatially nonuniform illumination.

When writing a grating with unexpanded light beams not only the longitudinal distribution of the light intensity is nonuniform (as discussed in pervious section) but also the strong transversal inhomogeneity appears because of Gaussian profile of intensity distribution of laser beams.

To minimize the effect of the transverse inhgomogeneity of light intensity distribution we measured the spectra of gain factor with the expanded writing beams. Total intensity of the input waves was about 100

mW/cm^2 and the transversal intensity variation was within 10% of the mean value.

The measured spectra for the expanded and unexpanded beams are shown in Fig.13 (by squares and diamonds respectively). The spectrum measured with the expanded beams still remains nonLorenzian. We doubt therefore that Gaussian shape of the recording beams is a main reason of unusual spectrum profiles.

2.3.3. Two-particle recombination.

The sharp nonexponential decay of a grating suggests the possibility of the high order recombination processes of photogenerated carriers. Two-partical and tree-partical (Auger) recombination usually manifest themselves at rather high densities of the photoexcited carriers when gratings are recorded by high power laser pulses [13,14]. It has been considered, however, also for CW excitation of sillenite crystals for the case when the density of empty traps is very small [15].

If two-particle recombination is dominating the free-carrier density is increasing in time as as hyperbolic tangent. Therefore the photoconductivity is also changing in time in different way, which results in a following function for the development of the refraction index change:

$$\Delta n(t) \propto (p / \gamma^{(2)}) \tanh\left(t\sqrt{p\,\gamma^{(2)}}\right), \qquad (11)$$

where p is the flux of photoexcitations and $\gamma^{(2)}$ is the probability of two-particle recombination.

The grating decay, on the opposite, is described by the modified hyperbolic function

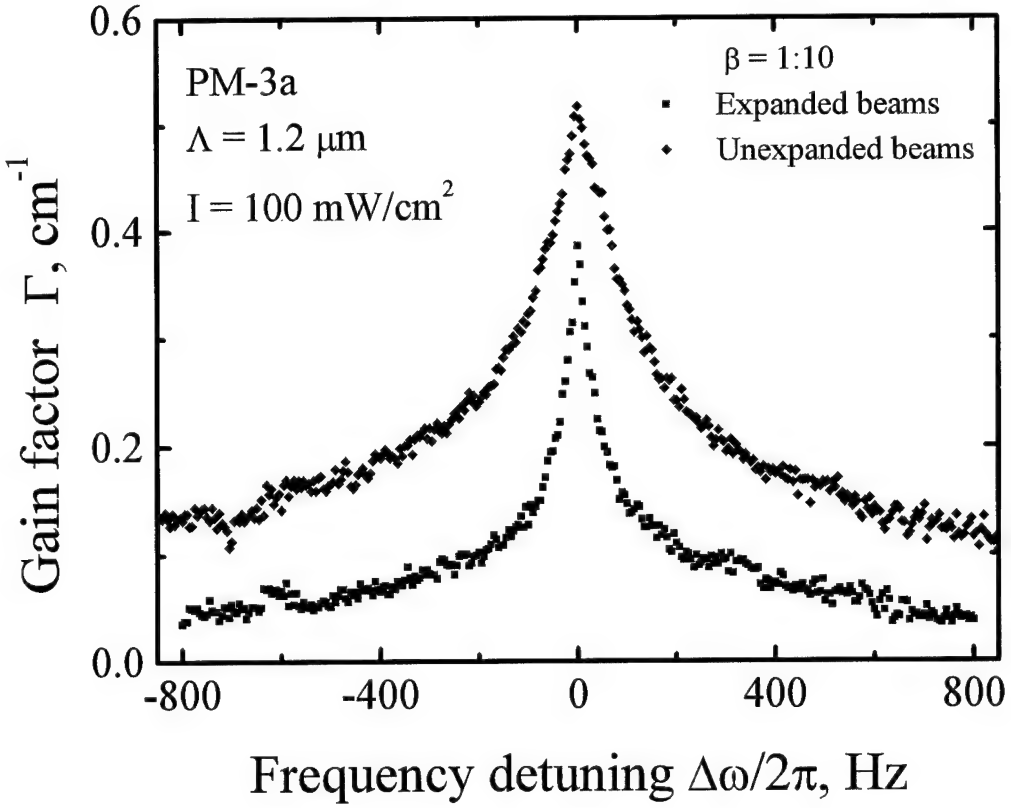
PM-3a
Λ = 1.2 μm
I = 100 mW/cm2
β = 1:10
Expanded beams
Unexpanded beams
Gain factor Γ, cm-1
0.0
0.2
0.4
0.6
-800
-400
0
400
800
Frequency detuning Δω/2π, Hz

Fig. 13.

$$\Delta n(t) \propto (p / \gamma^{(2)})\, t \sqrt{(p\,\gamma^{(2)}) + 1}\,. \qquad (12)$$

Figure 14a demonstrates the fit of the experimental data on grating decay to the dependence given by Eq.12. The agreement for this decay curve is reasonably good. Unfortunately, when we try to fit the build-up curve to Eq.11 using the same parameters $(p/\gamma^{(2)})$ and $(p\ \gamma^{(2)})$ as for Fig.14a we get completely different behavior as compared to the experimental curve (see solid line in Fig.14b).

Thus we conclude that the two-particle recombination can not explain the measured spectra and decay curves in our experimental conditions.

2.3.5. Amplitude gratings.

The unusual shape of spectra could result from the contribution of other (nonphotorefractive) gratings, e.g., from the amplitude gratings always existing in photorefractive crystals [16-18]. In case if amplitude gratings are strong enough to modify the spectra of photorefractive gratings there must appear the asymmetry of beam coupling: The amplification of one beam should not correspond to the depletion of the other. To check the possible difference we measure the spectrum of gain factor calculated from the depletion of the pump beam for different intensity ratios of the incident waves (see Fig.15a).

We measured, too, the spectra of the diffraction efficiency (Fig.15b) and dynamics of write-read cycle (Fig.16) with the probe beam counterpropagating to the recording beam I1 (and not counterpropagating to the beam I2 as in all previous cases).

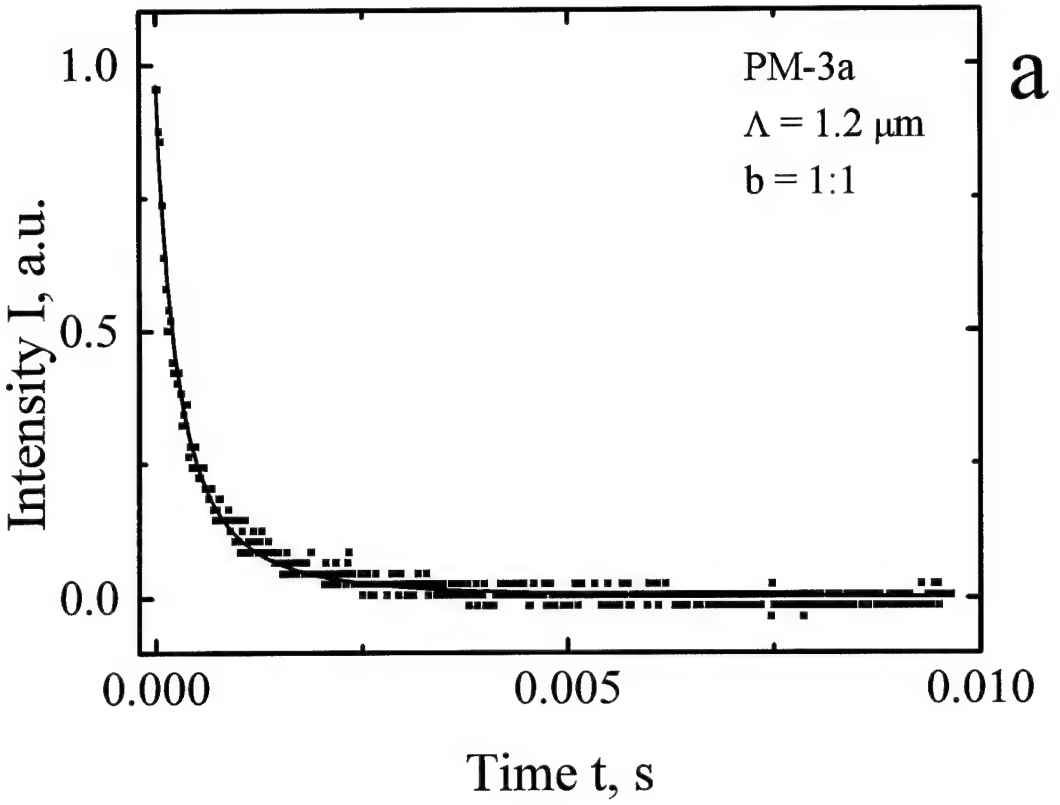
PM-3a
Λ = 1.2 μm
b = 1:1
a
Intensity I, a.u.
1.0
0.5
0.0
0.000
0.005
0.010
Time t, s

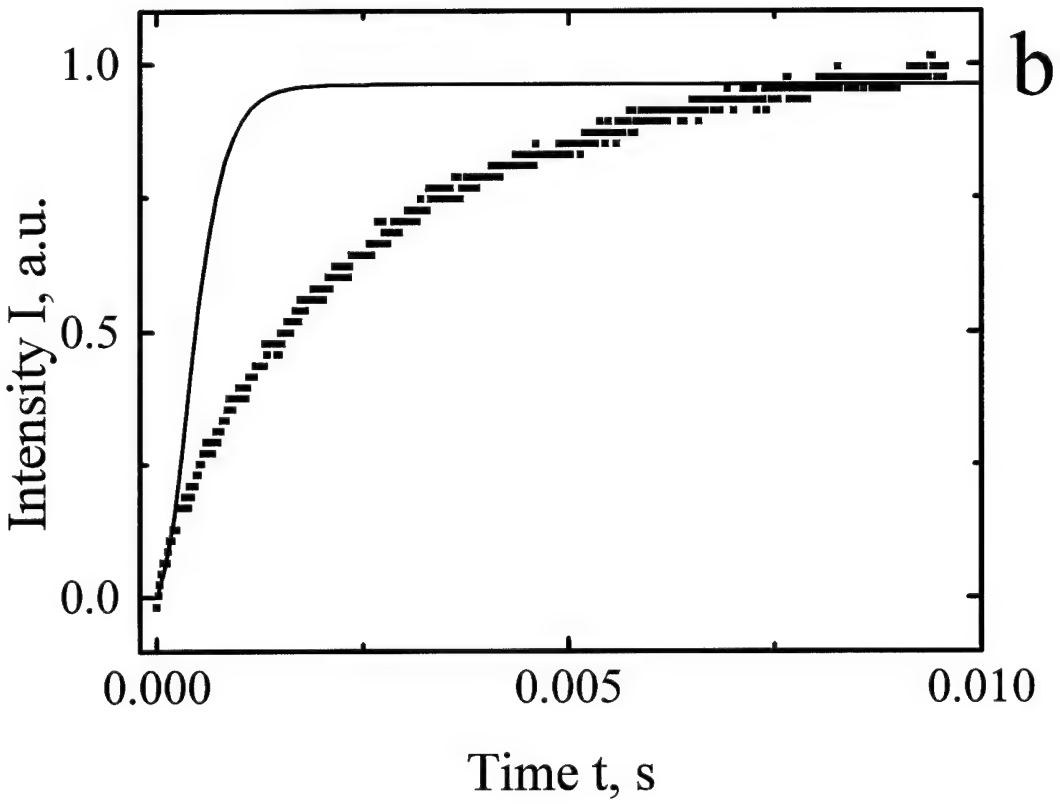
b
Intensity I, a.u.
1.0
0.5
0.0
0.000
0.005
0.010
Time t, s

Fig. 14.

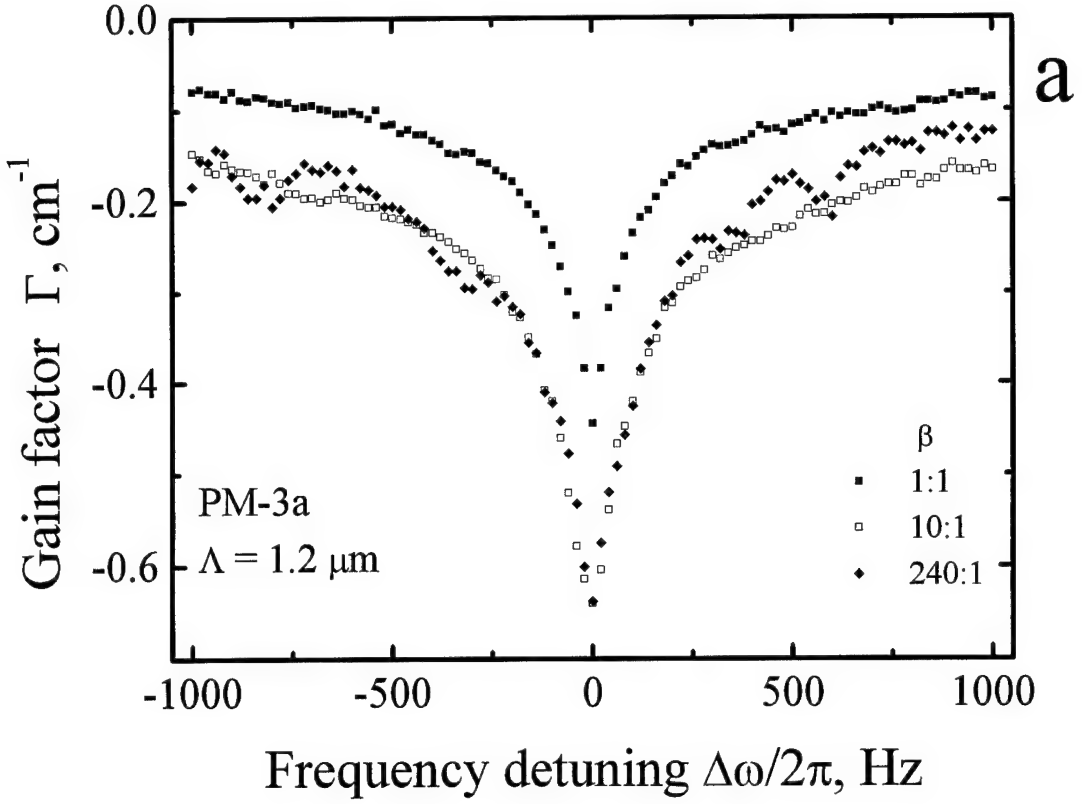
a
0.0
-0.2
-0.4
-0.6
Gain factor Γ, cm^{-1}
PM-3a
Λ = 1.2 μm
β
1:1
10:1
240:1
-1000
-500
0
500
1000
Frequency detuning Δω/2π, Hz

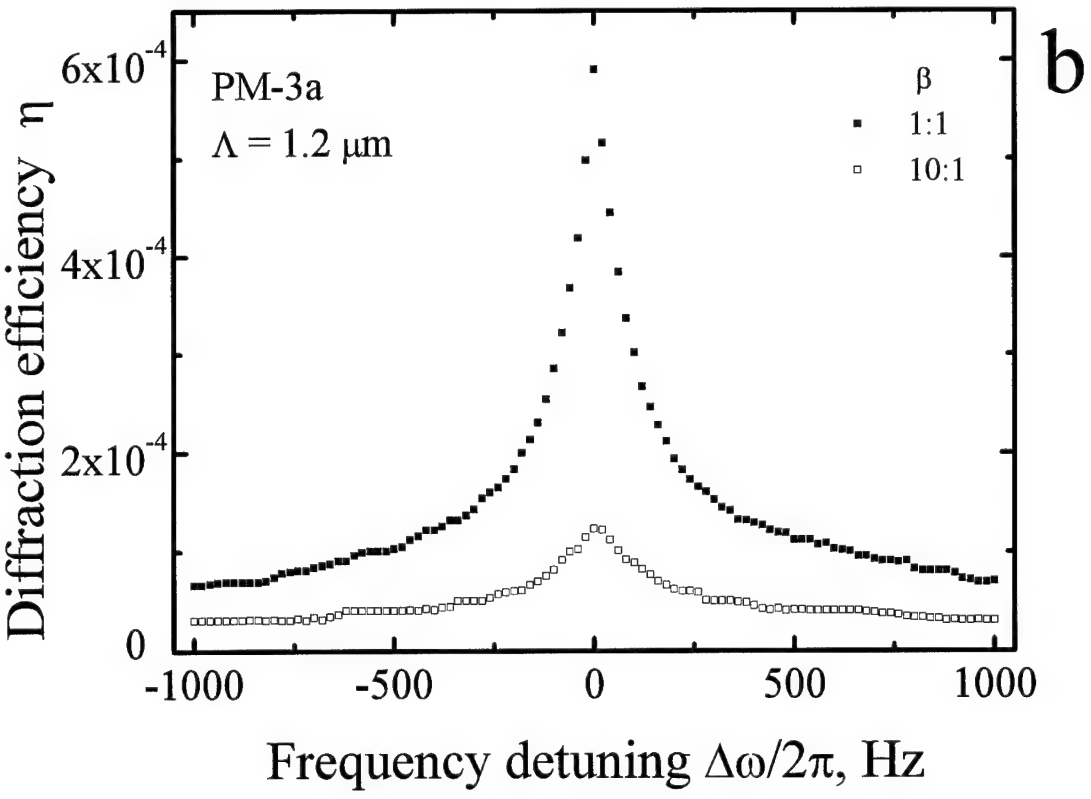
b
6x10^{-4}
4x10^{-4}
2x10^{-4}
0
Diffraction efficiency η
PM-3a
Λ = 1.2 μm
β
1:1
10:1
-1000
-500
0
500
1000
Frequency detuning Δω/2π, Hz

Fig. 15.

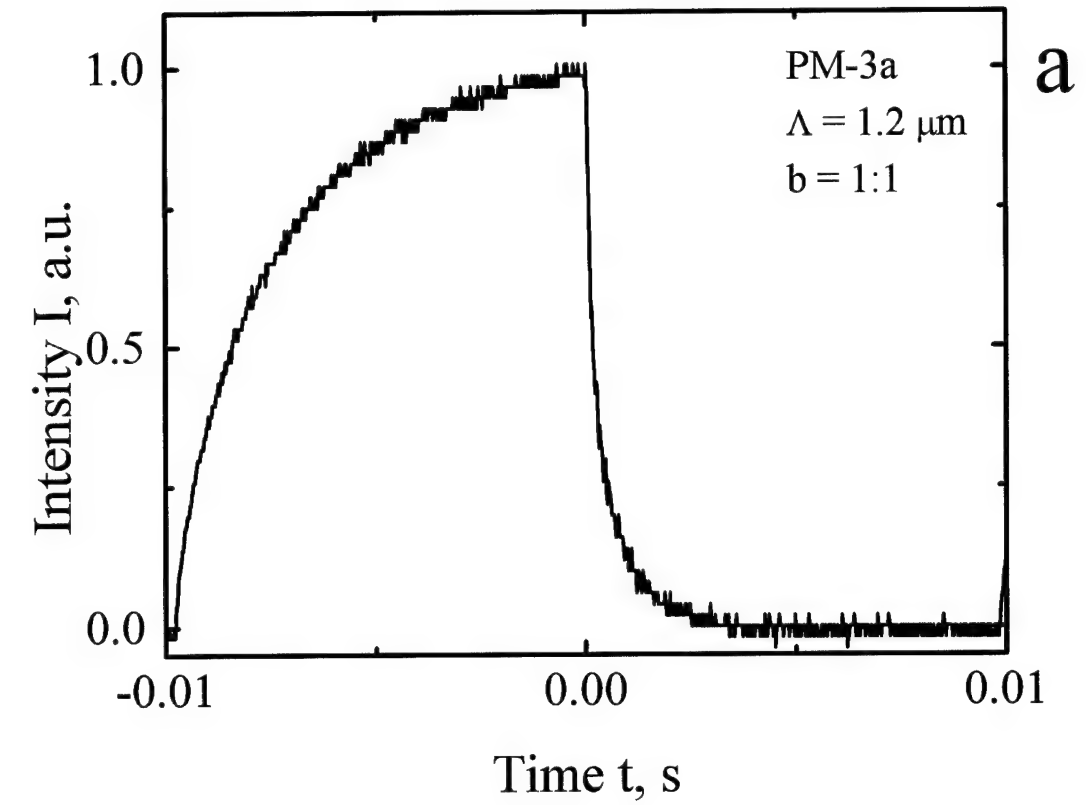
PM-3a
Λ = 1.2 μm
b = 1:1
a
Intensity I, a.u.
1.0
0.5
0.0
-0.01
0.00
0.01
Time t, s

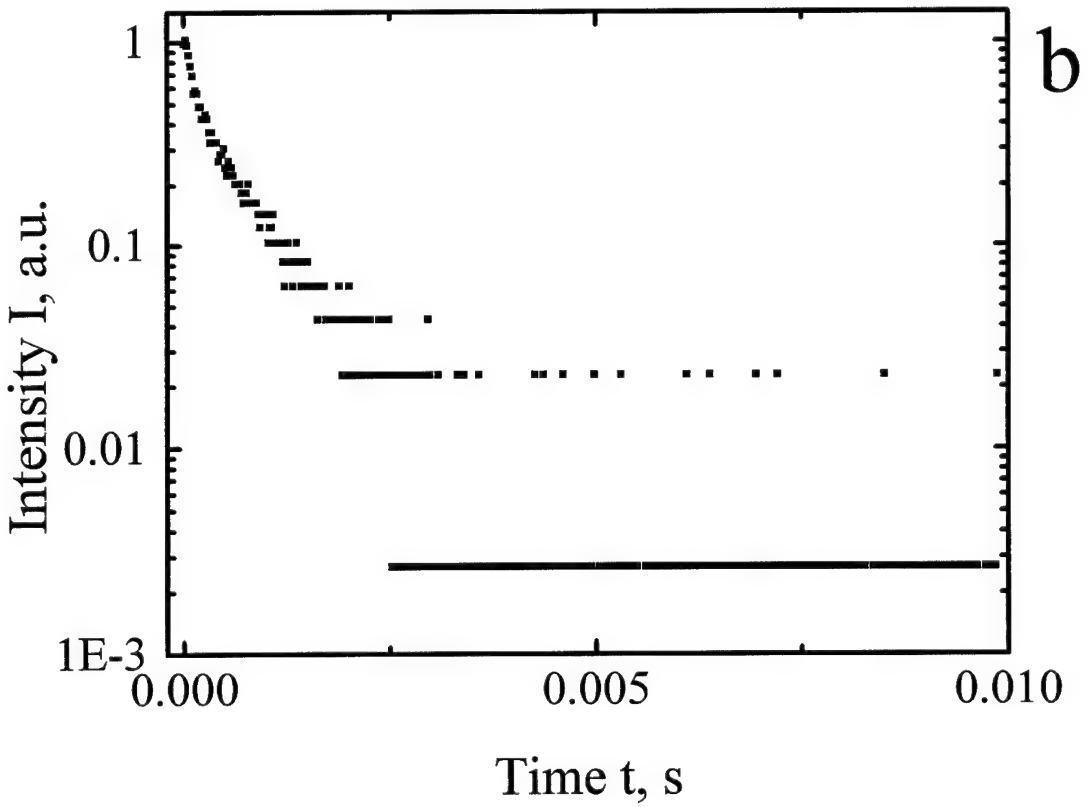
b
Intensity I, a.u.
1
0.1
0.01
1E-3
0.000
0.005
0.010
Time t, s

Fig. 16.

All the dependences measured in the conditions mentioned above are very similar to measured in standard geometry with only difference in sign of the gain factor. The spectra are nonLorenzian and the dynamics is nonexponential. From the similarity of the results for two writing waves we can conclude that there is no considerable contribution of the absorption grating to photorefractive recording.

2.3.5. Secondary centers (two-exponential decay).

A complicated shape of spectra can be explained by simultaneous recording of several (two or more) space charge gratings with different trap levels involved.

The integral spectra of the gain factor (or diffraction efficiency) in this case are the superposition (or square of the sum) of elementary Lorenz profiles. The temporal variation of the diffraction efficiency during optical erasure will also contain two (or several) exponents. Deviation from the exponential decay may indicate the presence of one (or several) secondary centers which become populated when crystal is illuminated by the recording waves [17,19].

In our previous experiments [6] because of limitations of the equipment used we detected only one (fastest) component in grating decay. With the electrooptic modulator (New Focus model 4004M) purchased for present experiments we were able to improve the accuracy of recording of the decay curve and to check the decay in wider range of intensities. This resulted in detection of deviations from single exponent behavior.

The study of the dynamics of the recording and erasure of the grating proved the asymmetry of the write-read cycles (see, e.g., Figs.9-11): When trying to fit the dynamics to single exponential process we get obviously different characteristic times of the recording and erasure. Fig.17a represents the log plot of the decay dynamics for the grating with Λ = 1.2 μm recorded by two beams of equal intensities in the sample PM-3a while Fig.17b shows the similar plot for the recording process with the time dependence of ln[1 - $I_{diff}(t)$]. The intensity was normalized to its maximum value so that η_0 was taken to be η_0 = 1.

The lines in these graphs shows the fit to single exponential decay

$$I = I_0 \exp(-t/\tau) \qquad (13)$$

with I_0 = 0.8 and τ = 470 μs for grating erasure and I_0 = 0.9 and τ = 2.6 ms for grating recording. If the grating build-up can be fitted to the single exponential function more or less satisfactory the decay is quite obviously strongly deviating from the single exponent. Note also that the characteristic times extracted in such a way from the recording and erasure curves differ nearly one order of magnitude in spite of the fact that for one center model they should be exactly the same.

Let us suppose that the grating recorded in the investigated CdTe samples consists of two independent photorefractive gratings with different amplitudes and different characteristic decay times. These gratings will enhance each other if they are formed by the carriers of the same sign or one of them will partially compensate the other if the carriers of opposite signs are involved in the recording of two gratings.

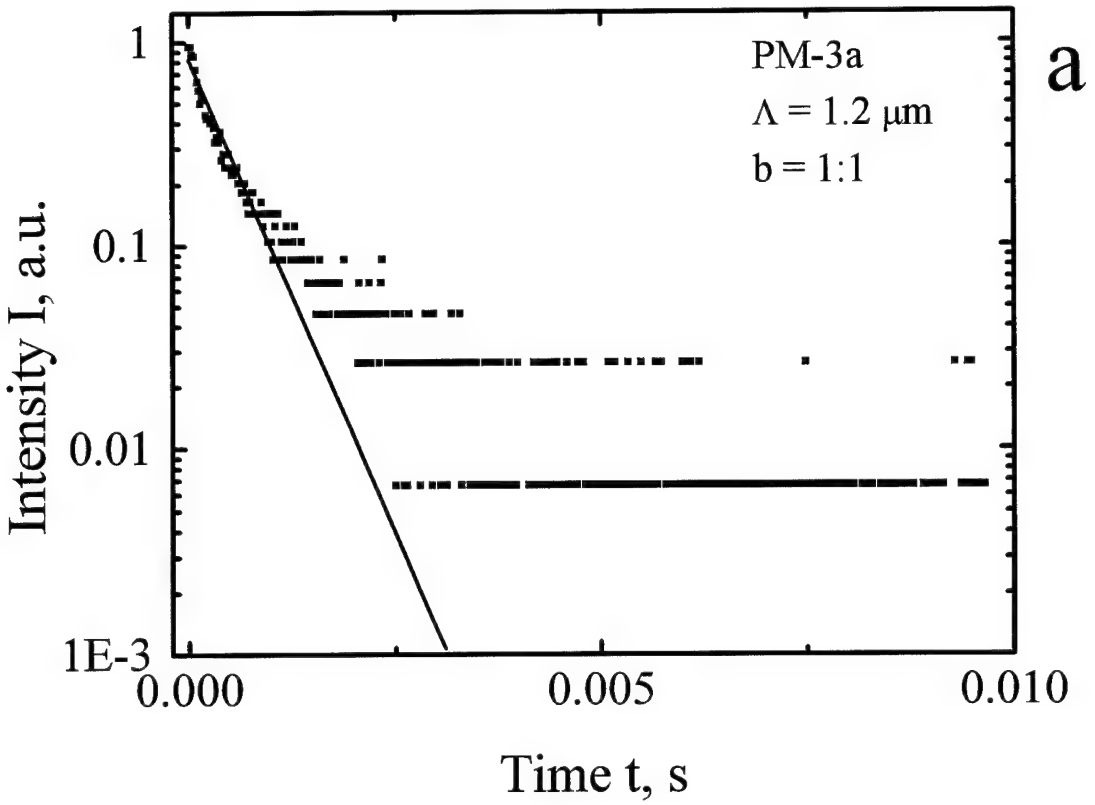
PM-3a
Λ = 1.2 μm
b = 1:1
a
Intensity I, a.u.
1
0.1
0.01
1E-3
0.000
0.005
0.010
Time t, s

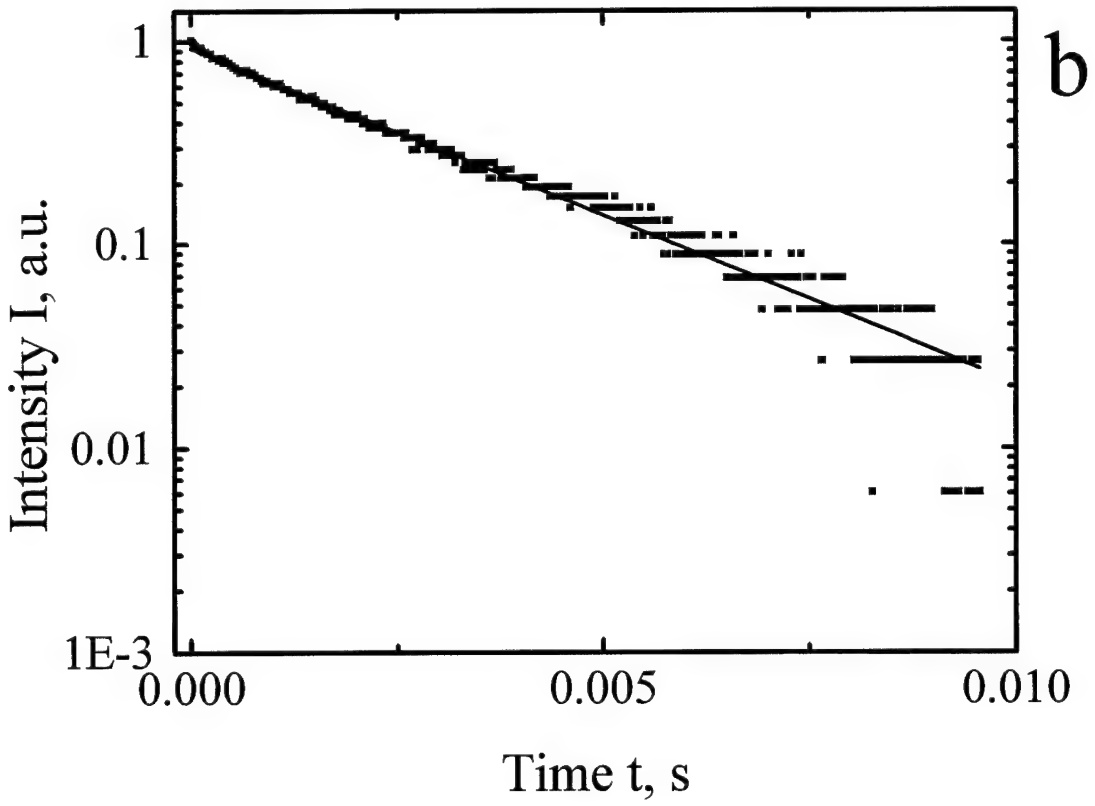
b
Intensity I, a.u.
1
0.1
0.01
1E-3
0.000
0.005
0.010
Time t, s

Fig. 17.

The integral intensity of the wave diffracted from this composite grating will be the square of the sum of particular contributions of two gratings. Then the temporal evolution of the integral diffraction efficiency during the grating erasure will be

$$\eta = \left(s\sqrt{\eta_0}\, \exp\left(-\frac{t}{\tau_1}\right) + (1-s)\sqrt{\eta_0}\, \exp\left(-\frac{t}{\tau_2}\right)\right)^2, \qquad (14)$$

where $\sqrt{\eta_0} = \sqrt{\eta_1} + \sqrt{\eta_2}$, $s = \dfrac{\sqrt{\eta_1}}{\sqrt{\eta_1} + \sqrt{\eta_2}}$, η_1, η_2 are the steady-state (saturated) values of the diffraction efficiency of the partial gratings and τ_1, τ_2 are their characteristic decay times, respectively.

For the recording process the diffraction efficiency can be represented in following manner

$$\eta = \left(\sqrt{\eta_0} - s\sqrt{\eta_0}\, \exp\left(-\frac{t}{\tau_1}\right) - (1-s)\sqrt{\eta_0}\, \exp\left(-\frac{t}{\tau_2}\right)\right)^2. \qquad (15)$$

When analyzing these formulae one can conclude that the same absolute change of the sum $[\eta_1(t) + \eta_2(t)]$ will affect more strongly the diffraction efficiency during the grating erasure because the relative change of the value to be squared is larger in this case. Therefore the decay of the grating should be faster than the recording.

Figure 18a,b shows by solid line the result of the fit of experimental data to the dependences 14,15. The extracted fit parameters are shown in the Table 2.

Both the data of Figure 18 and Table 2 demonstrate a rather good agreement of the measured data with the predictions of Eqs.14,15. This model

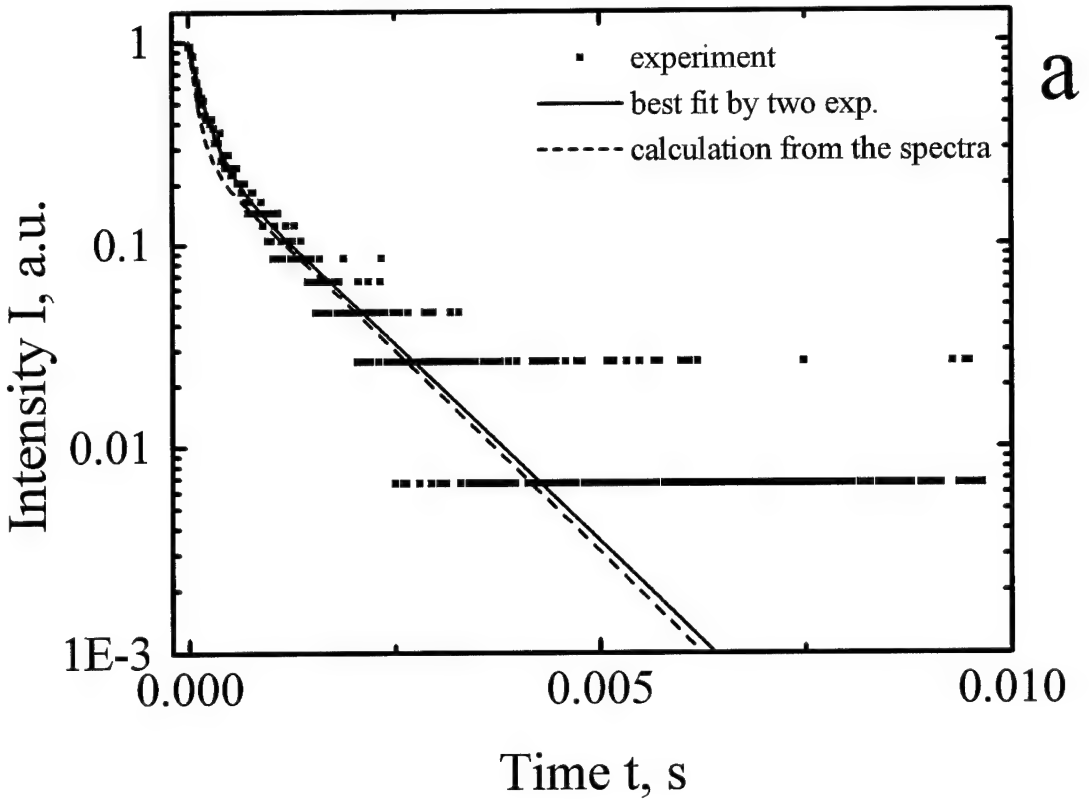
a
experiment
best fit by two exp.
calculation from the spectra
Intensity I, a.u.
1
0.1
0.01
1E-3
0.000
0.005
0.010
Time t, s

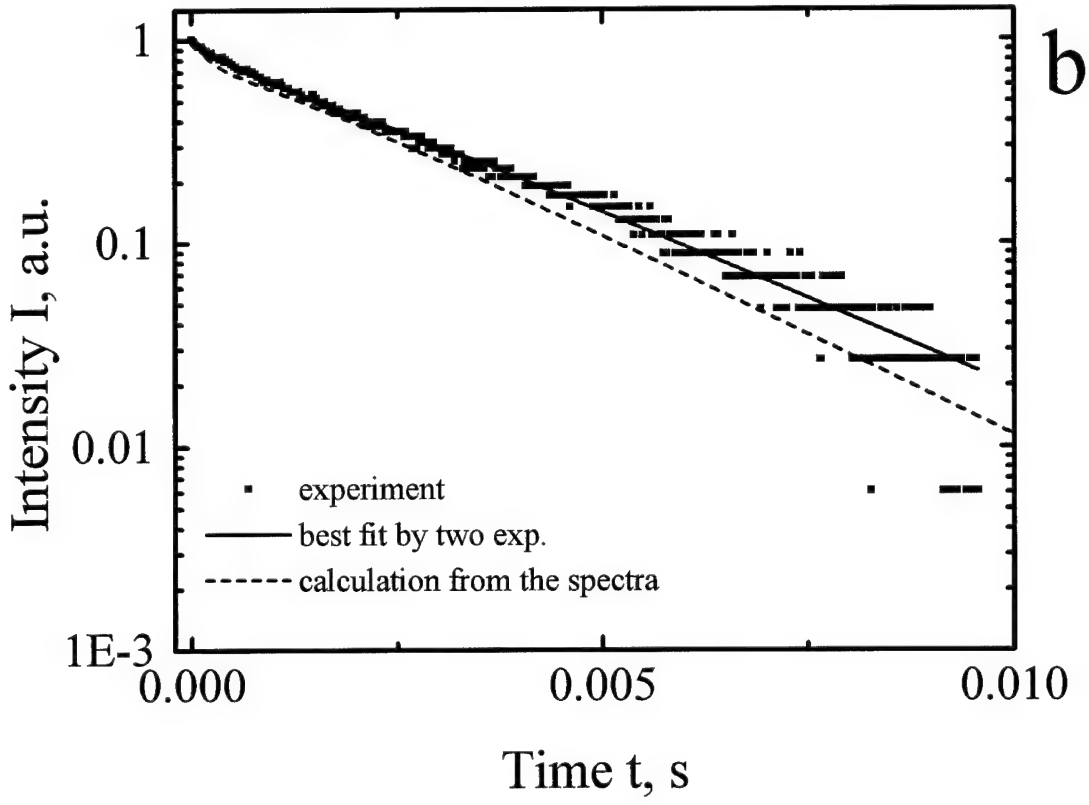
b
experiment
best fit by two exp.
calculation from the spectra
Intensity I, a.u.
1
0.1
0.01
1E-3
0.000
0.005
0.010
Time t, s

Fig. 18.

satisfactory describes not only nonexponential decay of the grating but also it suggests the explanation of the observed asymmetry of the write-read cycles.

Table 2.

	Erasure	recording
s	0.55	0.55
$\sqrt{\eta_0}$	1	1
τ_1 ms	2.2	2.5
τ_2 ms	0.23	0.24

In previous Report [6] we postulated that the integral gain factor for simultaneous recording of two gratings by waves with different temporal frequencies will be the sum of gain factors provided by partial gratings. The overall gain spectrum is

$$\Gamma = \frac{s\Gamma_0}{1+\Delta\varpi^2\tau_1^2} + \frac{(1-s)\Gamma_0}{1+\Delta\varpi^2\tau_2^2}, \qquad (16)$$

where $\Gamma_0 = \Gamma_1 + \Gamma_2$, $s = \frac{\Gamma_1}{\Gamma_1+\Gamma_2} = \frac{\sqrt{\eta_1}}{\sqrt{\eta_1}+\sqrt{\eta_2}}$, and Γ_1 and Γ_2 are the partial gain factors at strictly degenerate interaction.

The integral diffraction intensity for the considered case should be the square of the sum of amplitudes of two waves diffracted from partial gratings:

$$\eta = \left(\frac{s\sqrt{\eta_0}}{1+\Delta\varpi^2\tau_1^2} + \frac{(1-s)\sqrt{\eta_0}}{1+\Delta\varpi^2\tau_2^2} \right)^2 . \qquad (17)$$

In Fig.19 the spectra of gain (19a) and diffraction efficiency (19b) are shown, measured experimentally at exactly the same conditions as the

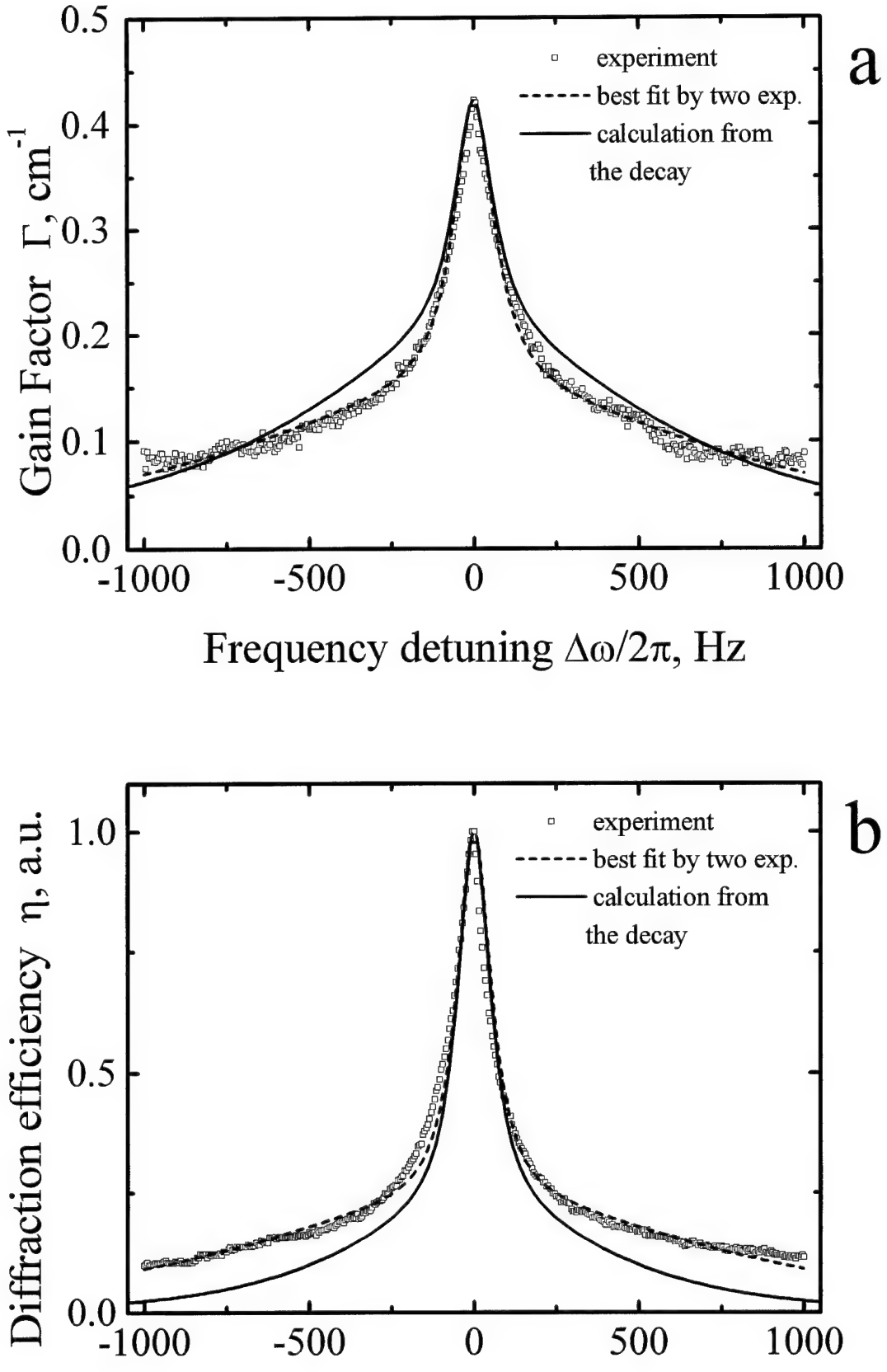
a
experiment
best fit by two exp.
calculation from the decay
Gain Factor Γ, cm-1
0.0
0.1
0.2
0.3
0.4
0.5
-1000
-500
0
500
1000
Frequency detuning Δω/2π, Hz
b
experiment
best fit by two exp.
calculation from the decay
Diffraction efficiency η, a.u.
0.0
0.5
1.0
-1000
-500
0
500
1000
Frequency detuning Δω/2π, Hz

Fig. 19.

dynamics of grating recording-erasure, considered above (Fig.17,18). The dashed lines in these spectra represent the best fit of the experimental data to Eqs.16 and 17. When extracting the fit parameters we use the value of Γ_0 = 0.42 cm^{-1} measured directly. The spectrum of the diffraction efficiency was normalized to its maximum value so that η_0 was taken to be η_0 = 1. The extracted fit parameters are presented in the Table 3.

Table 3.

	Gain spectra	Diffraction efficiency spectra
s	0.65	0.54
τ_1 ms	2.2	2.2
τ_2 ms	0.18	0.12

The solid lines in Fig.19a,b show the spectra of the gain factor and diffraction efficiency calculated from Eqs.16,17 with the fit parameters extracted from the direct measurements of the diffraction efficiency for grating erasure (Table 2). The results of calculation of dynamics with the parameters taken from the fit of the spectrum of the diffraction efficiency to Eq.17 (Table 3) are shown by dashed lines in figure 18.

To conclude, the decomposition of the grating build-up into two exponential processes allows for explanation of rather complicated experimental dependences obtained in direct measurements of temporal evolution of the diffraction efficiency and beam coupling. This decomposition

gives reasonable explanation to the shape of the gain and diffraction efficiency spectra.

At the same time we can not state for sure that the dynamics of photorefractive recording and erasure consists of formation of only two exponential processes. It could happen that much more complicated process involved in grating formation in semiconductor photorefractive crystals is satisfactory described by the proposed model.

As it has been already mentioned the other reasons for complicated dynamics (analyzed in this Report and not mentioned in it) could become dominant for the photorefractive crystals with parameters which differ from that typical to the investigated crystals.

3. Dynamic properties of drift-recorded gratings in CdTe.

The semiconductor crystals have much smaller electrooptic constants as compared to the wide bandgap ferroelectric crystals. Therefore the available values of the gain factor and diffraction efficiency are also much more modest. The improvement of these characteristics is possible by increasing of the space charge field when the recording takes place with the external electric field applied to the sample [20]. Two techniques of enhancement of photorefraction are known: In the first the AC field is applied when stationary (immobile) grating is recorded. In the second the moving fringes are recording the grating in the crystal with the DC field applied.

Our preliminary investigations [6] demonstrated that the recording of the grating in CdTe with AC electric field results in considerable increase of the characteristic time of recording. The practical implementation of this

technique faces considerable difficulties, too. The best results are obtained if the shape of the field variations is perfectly rectangular and the AC modulation frequency is higher than the reciprocal relaxation time of the grating [21]. Usually for semiconductors this frequency should be higher than 10 KHz. To design the high field generator keeping the rectangular shape of modulation at so high frequency is not an easy task.

The recording of the "moving" gratings in the DC field looks less difficult in spite of the fact that it requires a very uniform illumination of the sample. This was one reason why we decided to study the nearly degenerate two-beam coupling in crystals with the DC field. The second reason was related to the available equipment which we had already from our studies of gain and diffraction efficiency spectra.

In the experiments with DC field we found the same problem as when we were working with AC field: because of rather high conductivity the application of the electric field results in heating of the sample. For certain combination of voltage and light intensity the threshold of the thermal breakdown is overpassed and the resistance of the sample drops down in dramatic way. The larger is the light intensity the smaller becomes the threshold voltage of breakdown. For the sample PM-3a the threshold field without illumination was only 2 KV/cm. This limitation of allowable electric field was the main obstacle for getting high values of gain in ПМ-3a sample.

The other sample КТ-51-95 was selected for these experiments, its dark conductivity (10^{-9} Ohm $^{-1}$ cm $^{-1}$) being one order of magnitude smaller than for PM-3a (10^{-8} Ohm $^{-1}$ cm $^{-1}$). The threshold field for this sample illuminated with 200 mW/cm^2 light beam was about 7 KV/cm.

The spectra of the gain factor were measured for two-beam coupling with field and without field. The sample was illuminated with the expanded light waves; the deviation of the local intensity from the mean value was less than 10%. The profile of the measured spectra of the gain factor and diffraction efficiency was not Lorenzian as in the case of PM-3a sample.

The gain spectra measured for KT-51-95 sample with DC electric field E = 4 KV/cm at Λ = 2.1 μm are shown in Fig.20a and at Λ = 3.4 μm in Fig.20b. The filled squares show the dependence for beam intensity ratio β = 1:1 while open squares show the dependence for β = 1:10. The filled diamonds in this Figure mark the dependence for crystal with no field applied for β = 1:10.

The application of the external field to the sample affects the phase shift between the fringes and the grating of the refractive index. As one could expect this leads to transformation of the spectrum profile from the Lorenzian to the "dispersive".

As a reference we measured also the gain from the stationary grating in the same sample with the square shape AC field. The open diamonds in Fig.20 show the spectrum of gain; the X axis in this case represents the frequency of the AC field. At relatively small frequencies the transient beam coupling is observed with the amplification of the signal at doubled frequency as compared to the frequency of the external field. This transient amplification is shown in Fig.21. We calculated the gain factor taking into account the largest value of the signal wave intensity which is due to the transient gain.

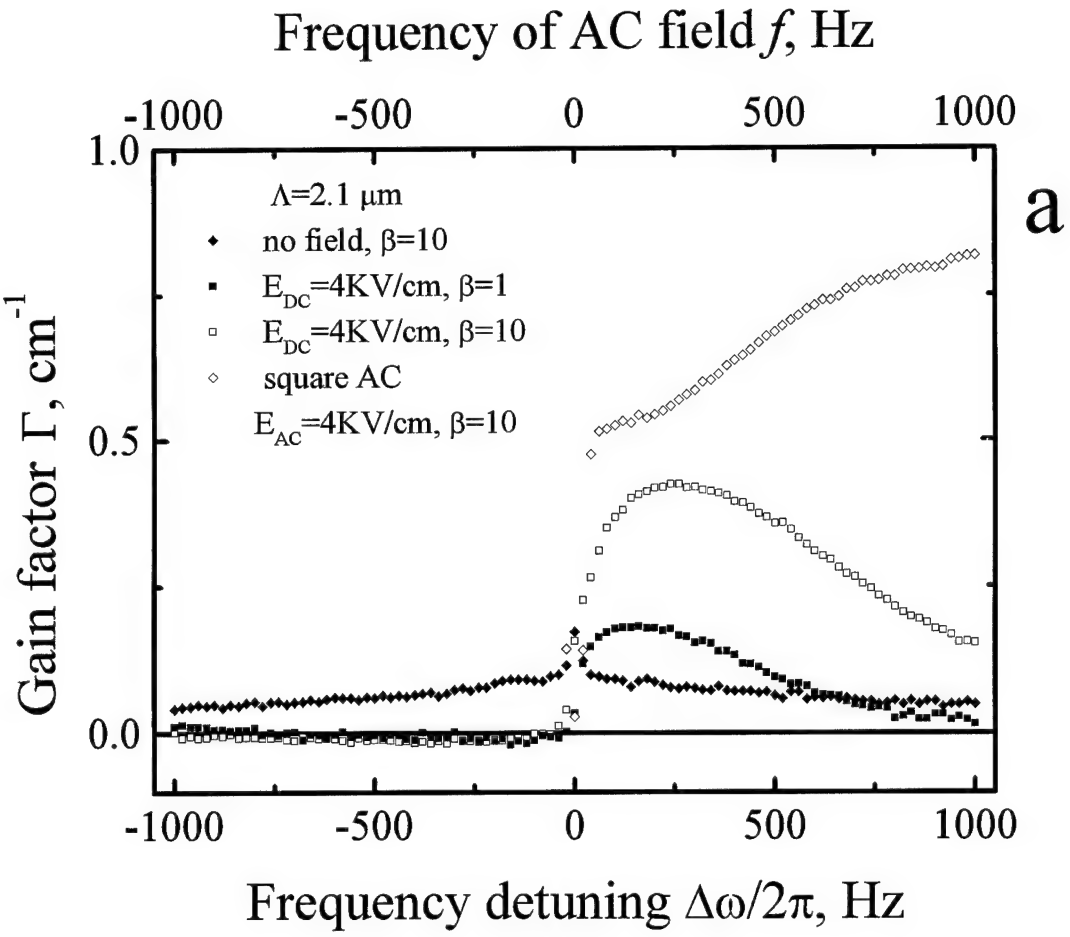
Frequency of AC field f, Hz
-1000
-500
0
500
1000
1.0
0.5
0.0
Gain factor Γ, cm-1
Λ=2.1 μm
no field, β=10
EDC=4KV/cm, β=1
EDC=4KV/cm, β=10
square AC
EAC=4KV/cm, β=10
a
Frequency detuning Δω/2π, Hz

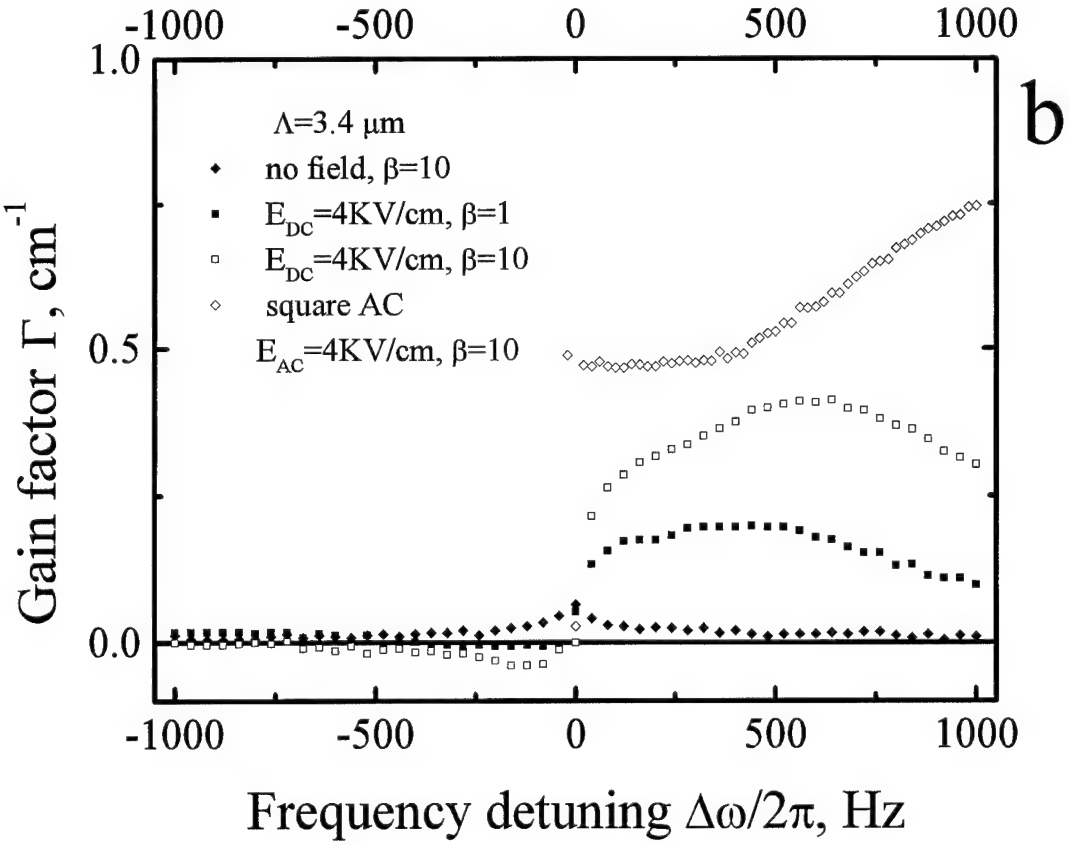
Frequency of AC field f, Hz
-1000
-500
0
500
1000
1.0
0.5
0.0
Gain factor Γ, cm-1
Λ=3.4 μm
no field, β=10
EDC=4KV/cm, β=1
EDC=4KV/cm, β=10
square AC
EAC=4KV/cm, β=10
b
Frequency detuning Δω/2π, Hz

Fig. 20.

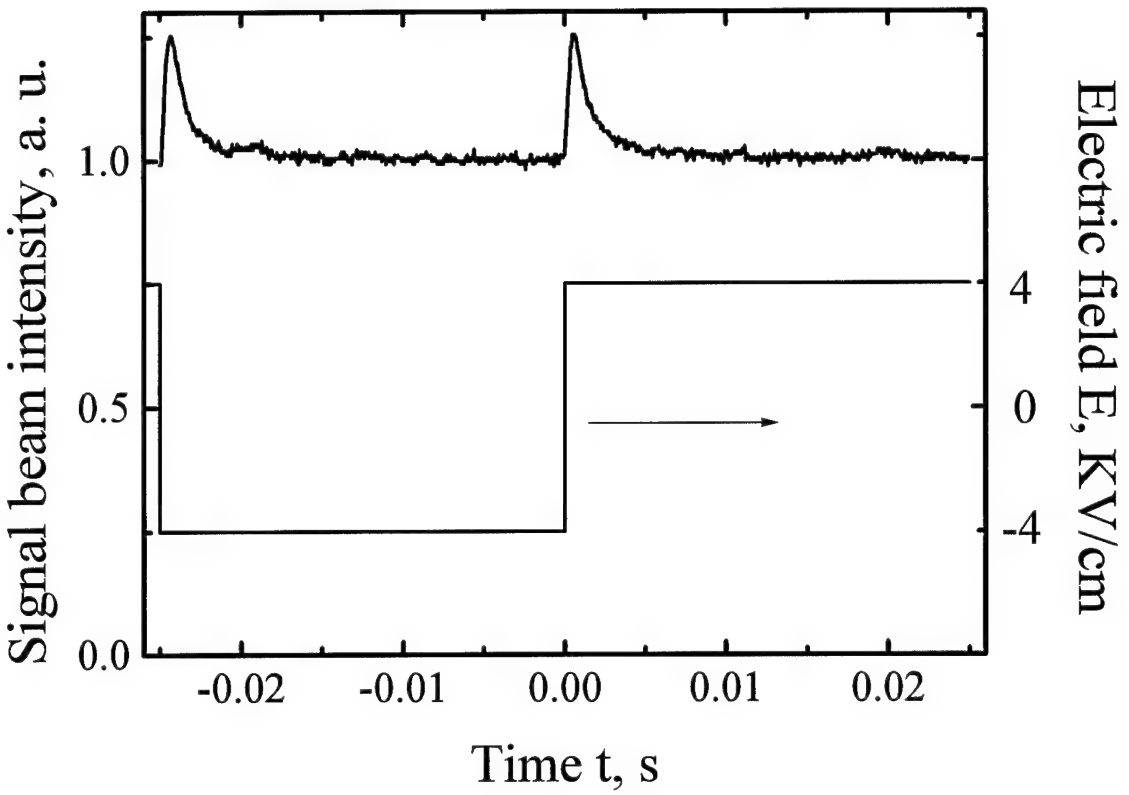
Signal beam intensity, a. u.
1.0
0.5
0.0
-0.02
-0.01
0.00
0.01
0.02
Time t, s
Electric field E, KV/cm
4
0
-4

Fig. 21.

With the increase of the AC field frequency to the values larger than the reciprocal width of transient spiking the contrast of intensity modulation of the signal wave vanishes to zero and the amplification saturates at a certain value.

The data of Fig.20 show that the use of AC field with CdTe crystals gives the larger gain factors. However, the disadvantage of this technique is in considerable intensity modulation of the amplified signal beam at frequencies up to 1 KHz. This can create the problems when amplifying, e.g., the AM signals. In addition, for shorter relaxation times (larger intensity or larger grating spacings) the square shape AC field is necessary with the frequency larger than 1 KHz what is difficult to realize technically.

4. Gain spectra for crystals with bipolar conductivity.

To describe the dynamics of photorefractive grating recording in CdTe we use the model incorporating the development of two gratings, each with its own amplitude and its own lifetime. One possible version of such a recording is the recording in crystals with two types of movable charge carriers, i.e. with electrons and holes. This is why the calculation of the dynamics of nearly degenerate two-beam coupling in photorefractive crystal possessing two types of movable charge carriers has been performed.

4.1. Calculation of gain factor.

The detailed description of mathematical procedure is given in the manuscript [22] prepared for publication (see Attachment). Here only a short summary is given and the principal results are presented.

In given-field approximation, i.e., considering the material equations for photorefractive crystal only, we got an analytic solution for temporal behavior of the space-charge field. This allowed us to calculate the gain factor and finally the intensity of the amplified weak beam as a function of time. The spectra of the transient gain factor and steady-state gain factor were found to compare with the experimental results.

It has been shown that in the range of frequency detuning between the reciprocal relaxation time of the "slow" grating and reciprocal relaxation time of the "fast" grating the steady-state gain factor reaches the maximum value close to the pick value of transient gain.

Some other important results of calculation should be mentioned: The temporal evolution of weak beam intensity exhibits in general case a sharp increase followed by slow decay with damped oscillations. The frequency of these oscillations was shown to be equal to the frequency detuning between two incident waves.

Figures 22 and 23 show the calculated dynamics of the weak beam intensity and the gain factor spectrum, respectively. The set of parameters used in this particular computer simulation was taken from our experimental data for new infrared-sensitive photorefractive crystal, tin hypothiodiphosphate ($Sn_2P_2S_6$). In Fig.22 the calculated dynamics (left row) can be compared with the directly measured (right row). An exelent agreement of two sets is obvious. In Fig.23 the calculated data (solid lines) are also compared with the measured (dots).

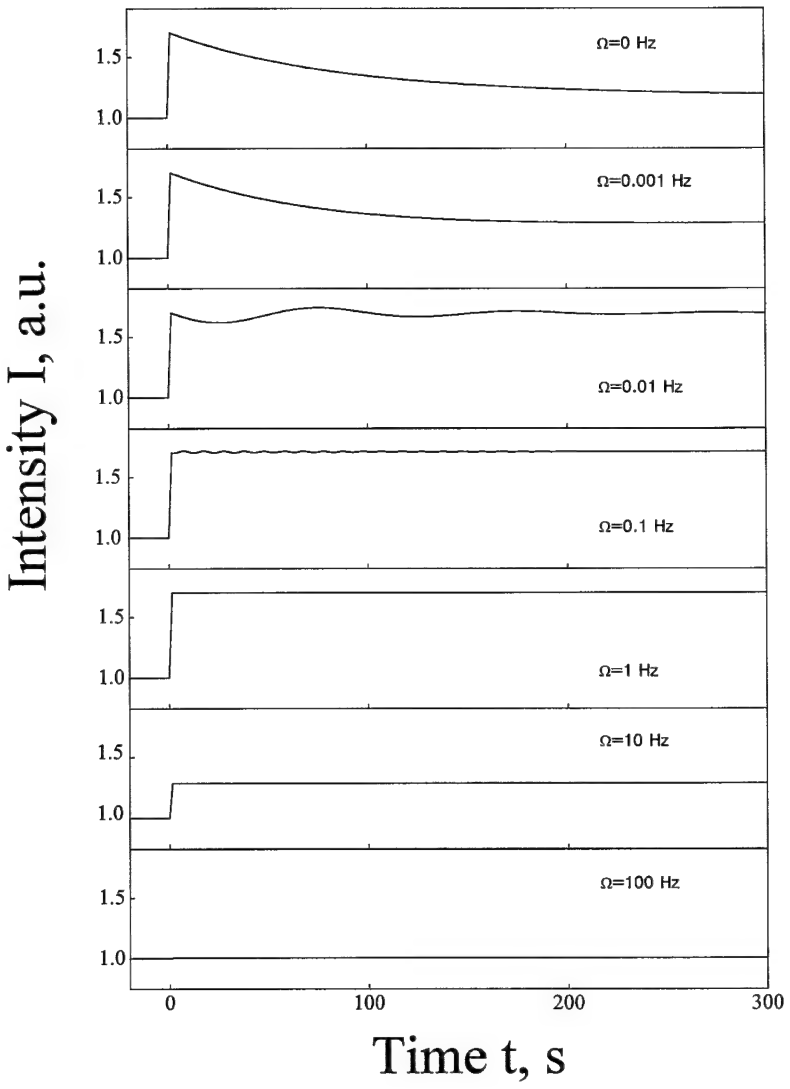
Intensity I, a.u.
Ω=0 Hz
Ω=0.001 Hz
Ω=0.01 Hz
Ω=0.1 Hz
Ω=1 Hz
Ω=10 Hz
Ω=100 Hz
1.5
1.0
0
100
200
300
Time t, s

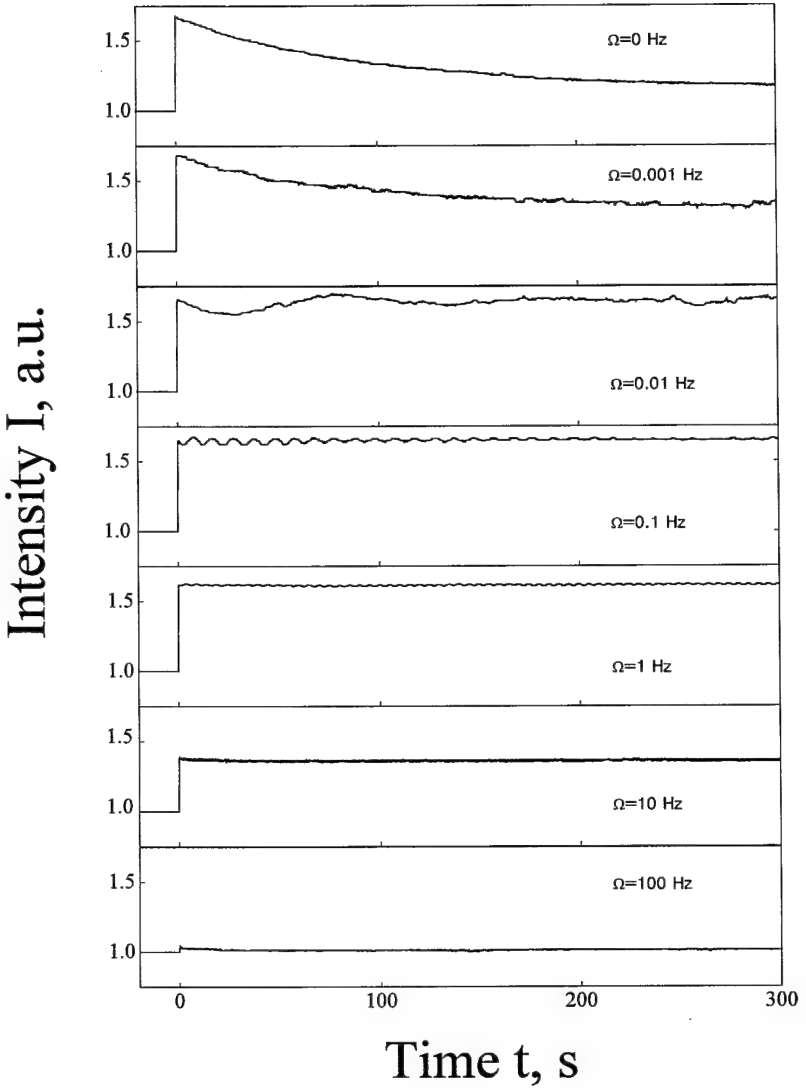
Intensity I, a.u.
Ω=0 Hz
Ω=0.001 Hz
Ω=0.01 Hz
Ω=0.1 Hz
Ω=1 Hz
Ω=10 Hz
Ω=100 Hz
1.5
1.0
0
100
200
300
Time t, s

Fig. 22.

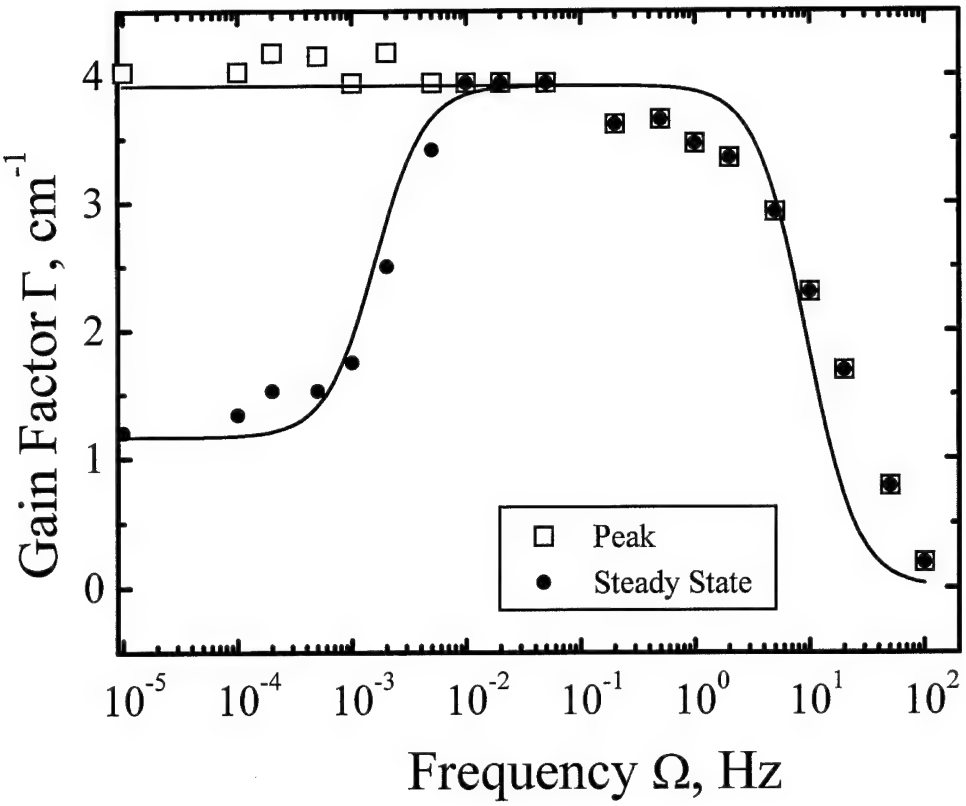
Gain Factor Γ, cm^{-1}
4
3
2
1
0
Peak
Steady State
10^{-5}
10^{-4}
10^{-3}
10^{-2}
10^{-1}
10^{0}
10^{1}
10^{2}
Frequency Ω, Hz

Fig. 23.

4.2. Manifestation of bipolar conductivity in CdTe.

We observed the similar gain spectra with the deep at zeroth detuning frequency also in two samples of CdTe crystal (N3 and PM-2, see Fig.24, 25, respectively); for the other sample (PM-1a) the deep was not resolved but the obvious flattening of the maximum of gain spectrum was clearly visible (see Fig.26). These data are interpreted as the manifestation of the electron-hole competition in the formation of the space charge grating.

The deep observed in the gain spectrum of the sample N3 may be related to bipolar conductivity of the sample. To check this hypothesis we measure the dynamics of the signal beam intensity (when this beam is amplified or depleted). The relevant temporal dependences are shown in Fig.27 (sign "+" for amplification and "-" for depletion). At first intensity of the signal wave is quickly increasing (decreasing) reaching the maximum (minimum) value and than slowly approaches the steady-state value. Curves for amplification and depletion are nearly symmetric; this symmetry points to the diffusion process of grating recording within a whole transient period of recording. Thus we believe that at first the grating is recorded by the redistribution of carriers of one sign and than this grating is partially compensated by the grating formed by the carriers of opposite sign.

The dynamics of the beam coupling in zeroth approximation can be represented in following way:

$$I_S = I_{S0} + I_1\left[1 - \exp\left(-\frac{t}{\tau_1}\right)\right] + I_2\left[1 - \exp\left(-\frac{t}{\tau_2}\right)\right], \qquad (18)$$

where I_1 and I_2 are the steady-state values the output signal intensity would have if only the first or only the second grating are recorded; τ_1 and τ_2 are

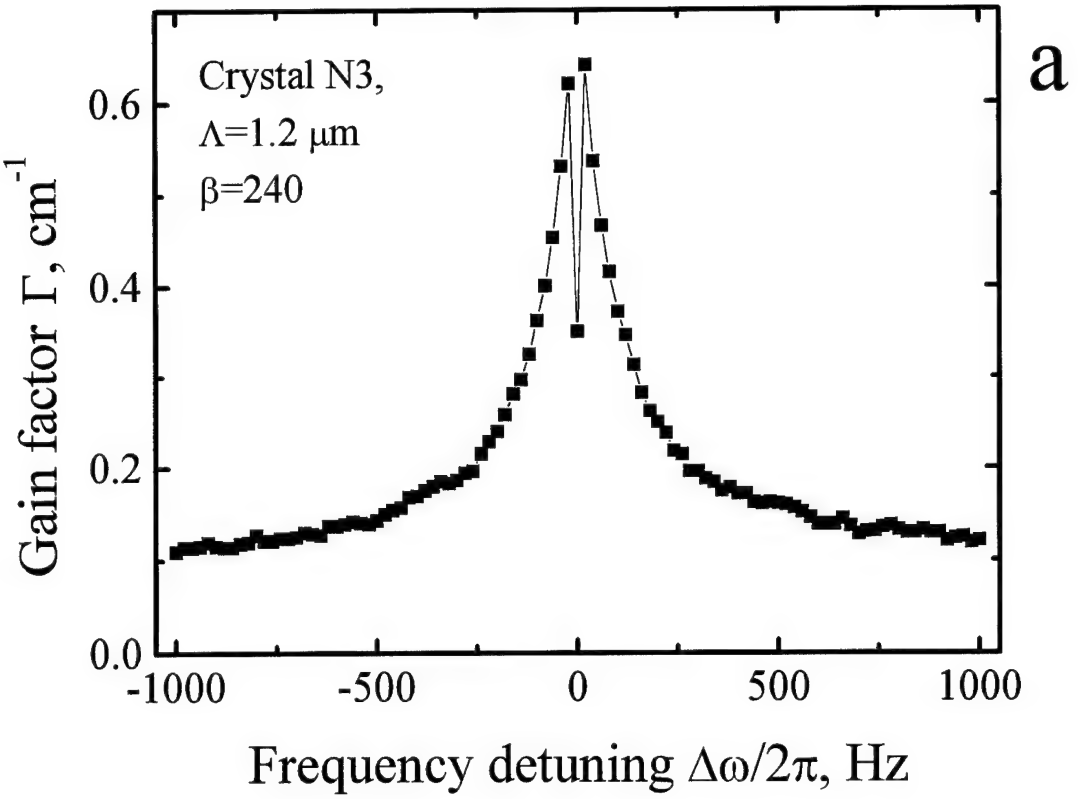
a
Crystal N3,
Λ=1.2 μm
β=240
Gain factor Γ, cm-1
0.0
0.2
0.4
0.6
-1000
-500
0
500
1000
Frequency detuning Δω/2π, Hz

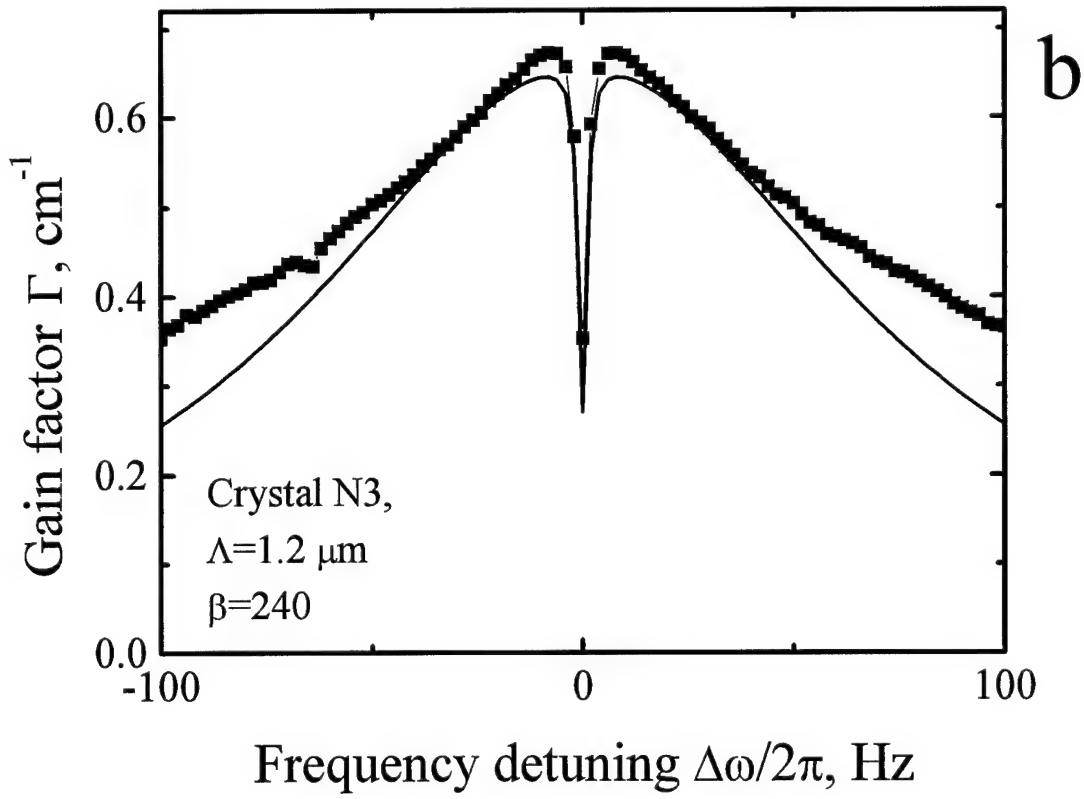
b
Crystal N3,
Λ=1.2 μm
β=240
Gain factor Γ, cm-1
0.0
0.2
0.4
0.6
-100
0
100
Frequency detuning Δω/2π, Hz

Fig. 24.

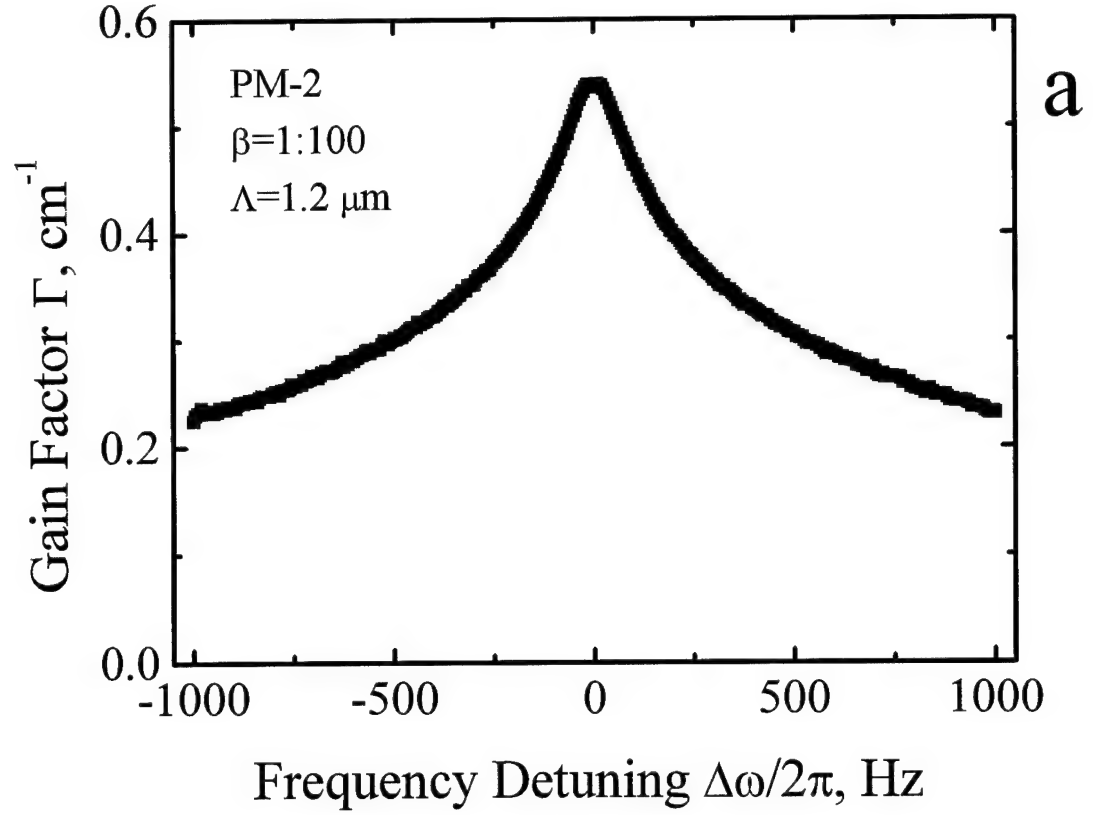
PM-2
β=1:100
Λ=1.2 μm
a
Gain Factor Γ, cm-1
0.6
0.4
0.2
0.0
-1000
-500
0
500
1000
Frequency Detuning Δω/2π, Hz

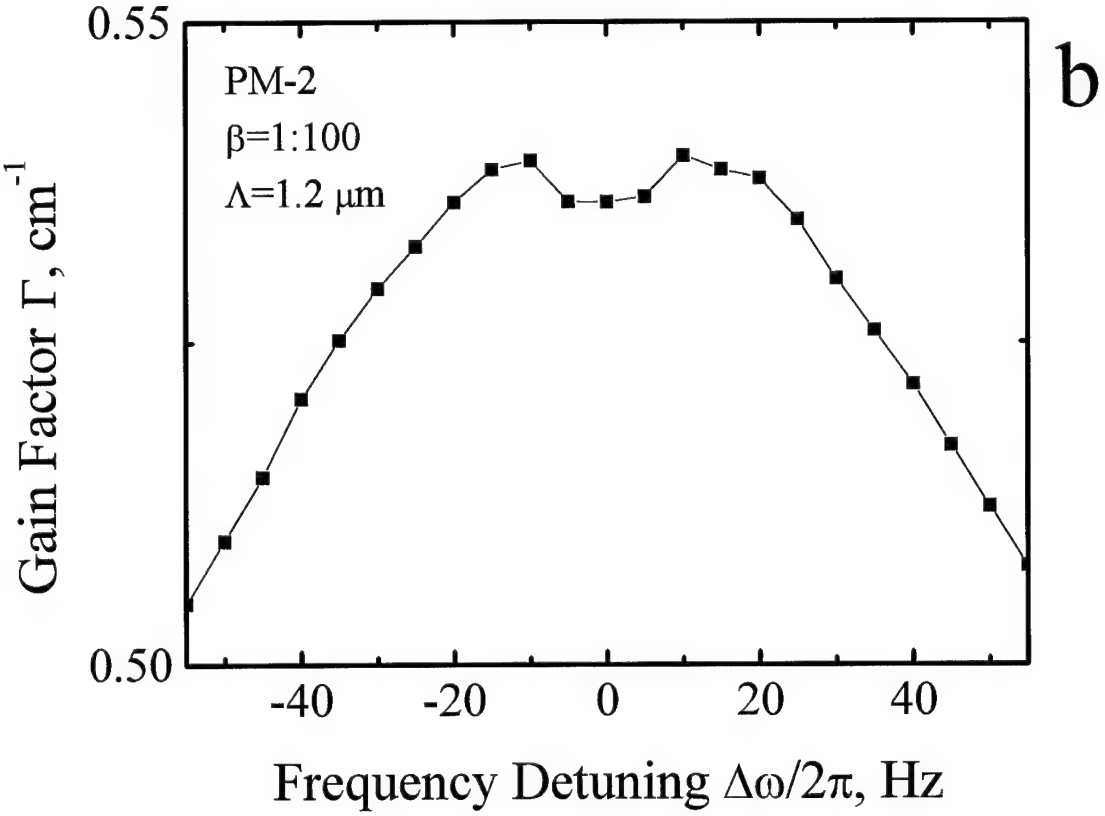
PM-2
β=1:100
Λ=1.2 μm
b
Gain Factor Γ, cm-1
0.55
0.50
-40
-20
0
20
40
Frequency Detuning Δω/2π, Hz

Fig. 25.

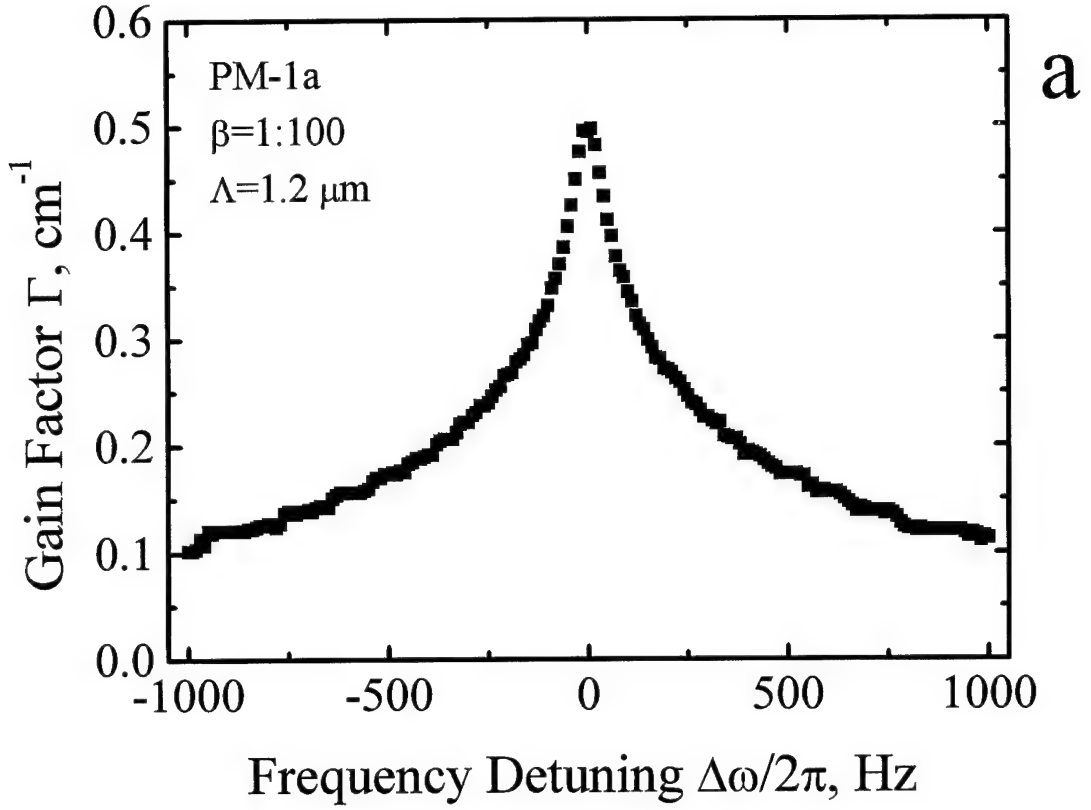
PM-1a
β=1:100
Λ=1.2 μm
Gain Factor Γ, cm-1
0.6
0.5
0.4
0.3
0.2
0.1
0.0
-1000
-500
0
500
1000
Frequency Detuning Δω/2π, Hz

a

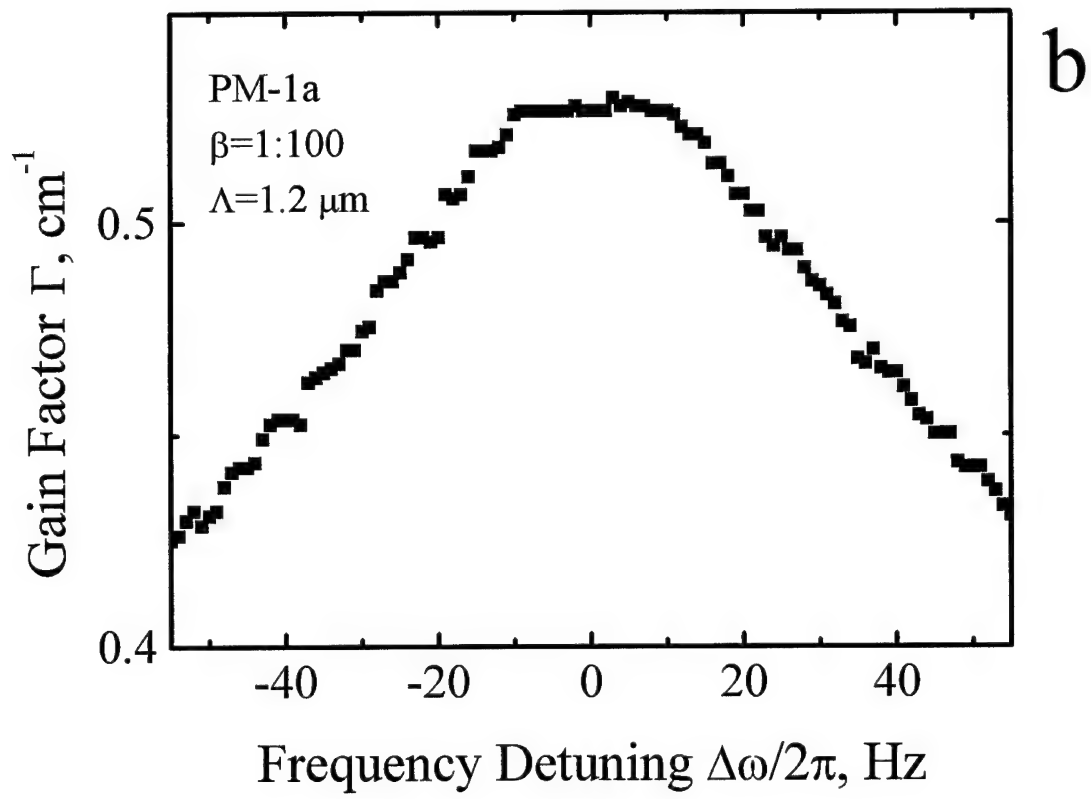
PM-1a
β=1:100
Λ=1.2 μm
Gain Factor Γ, cm-1
0.5
0.4
-40
-20
0
20
40
Frequency Detuning Δω/2π, Hz

b

Fig. 26.

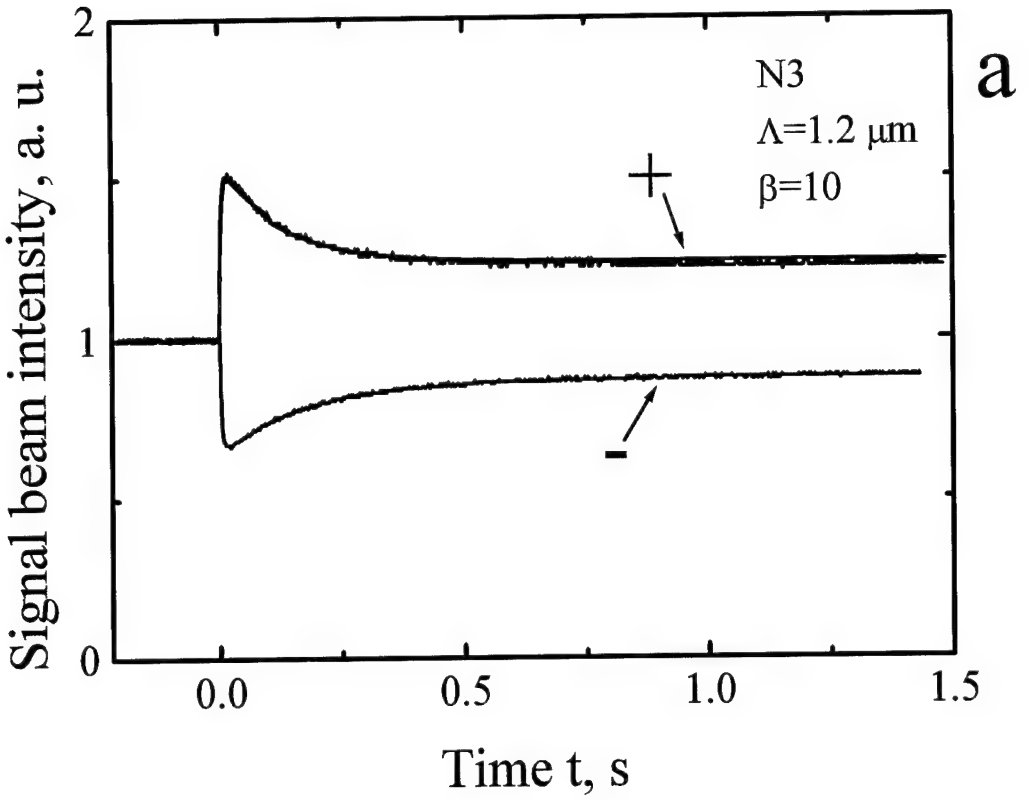
a
N3
Λ=1.2 μm
β=10
+
-
Signal beam intensity, a. u.
Time t, s
0
1
2
0.0
0.5
1.0
1.5

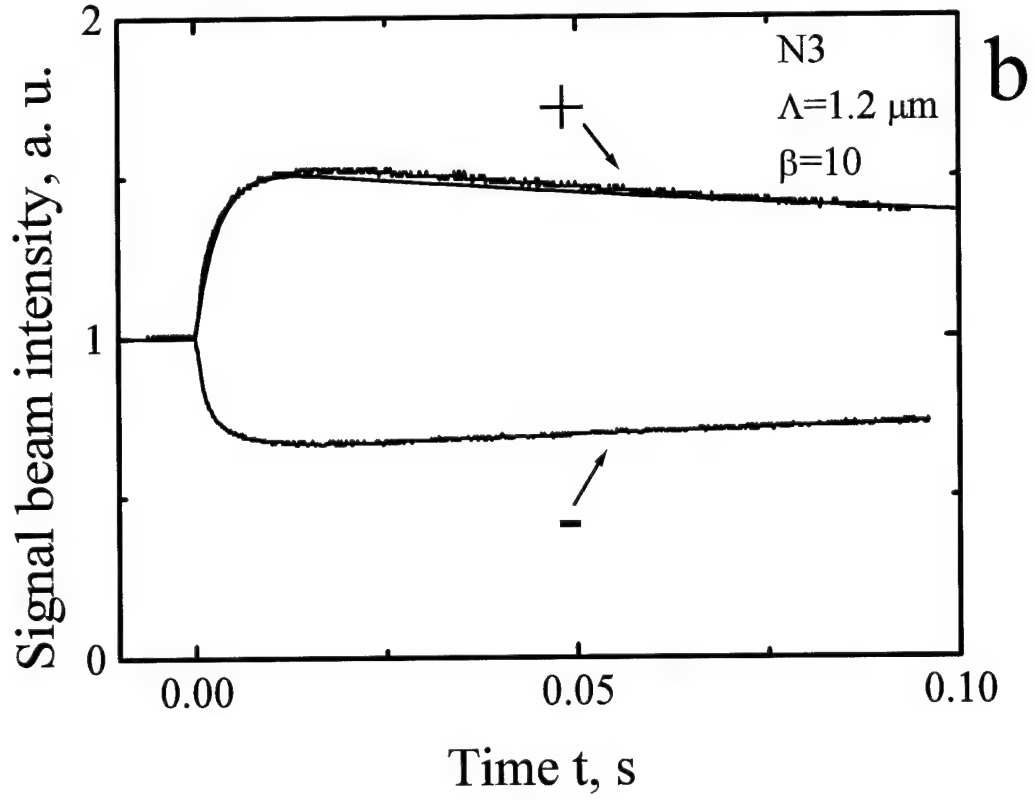
b
N3
Λ=1.2 μm
β=10
+
-
Signal beam intensity, a. u.
Time t, s
0
1
2
0.00
0.05
0.10

Fig. 27.

the gratings relaxation times. Labeling the faster grating as "1" we can extract from data of Fig.27:

$I_1 = I_{max} - I_{S0}$,

$I_2 = I_{Sat} - I_{max}$,

$\tau_1 = \tau_{sum}$ if $t \rightarrow 0$,

$\tau_2 = \tau_{sum}$ if $t >> \tau_1$,

where I_{Sat} is the steady-state (saturated) value of the output signal wave intensity and τ_{sum} is the exponential decay time for relevant time interval of the dynamics curve.

Figure 27 shows the fit of experimental dynamics to dependence given by Eq.18 (solid line). The fitting parameters are τ_1 = 3 ms, τ_2 = 133 ms, I_1 = 0.5, I_2 = -0.26.

The gain spectrum will be given Eg.16. The values Γ_1 = 0.66 cm^{-1} and Γ_2 = - 0.27 cm^{-1} may be calculated from I_1 and I_2. As the gain factors Γ_1 and Γ_2 here have different signs |s| becomes larger than unity, s = 2,4.

The spectrum calculated from Eq.16 with the parameters extracted from the fit of the beam coupling dynamics to Eq.18 is shown by the solid line in Fig.24b. For relatively small frequency detuning ($|\Delta\omega/2\pi| \leq$ 30 Hz) not only a qualitative but a quantitative agreement is evident.

Note that the maximum gain factor $\Gamma \approx$ 0.67 cm^{-1} can be reached in sample N3 at relatively small ($\Delta\omega/2\pi \approx$ 6 ... 8 Hz) frequency detuning. The enhancement factor is rather high reaching nearly 2.5 times. This could be interesting for such practical application as a design of the Bandpass Novelty Filter [23].

Conclusions

The research performed in accordance with the Workplan of present Project shows that the dynamics and the spectra of photorefractive gratings recorded in semiinsulating cadmium telluride can not be described by a simple model of the space charge grating formation with one type of free carriers and one traps level. Both the temporal behavior of grating build-up and erasure and the shape of spectra deviate from the predicted by the theory for this elementary model.

We analyzed some possible reasons of observed deviation and show that for crystals we use nether the absorption or nonuniform illumination of the crystal nor the absorption grating or two-particle recombination can change the measured spectra so dramatically. We propose the model which describes the experimental results both for dynamics and spectra taking the assumption that the process of the grating formation consists of two simple exponential processes. Within this assumption a perfect agreement of measured spectral and temporal behavior of photorefractive gratings recorded in cadmium telluride exists.

The study of the "moving" grating recorded in cadmium telluride in DC electric field has been fulfilled. The results obtained show that for semiinsulators (crystals with very strong screening of the electric field) the improvement of the gain factor is mach larger for the rectangular AC field than for DC case. On the other hand there are some advantages of the DC field related to the absence of modulation of intensity with doubled frequency of the field and to technical simplicity.

As we use the theoretical model taking into account two elementary processes we performed the calculation of the dynamics of nearly degenerate two-beam coupling in photorefractive crystal possessing two types of movable charge carriers. The results of this calculation are in perfect agreement with experimental results for tin hypothiodiphosphate ($Sn_2P_2S_6$) which is characterized by the bipolar conductivity.

The gain spectra with the deep at zeroth detuning frequency are observed in some cadmium telluride crystals. These data manifest the strong electron-hole competition in the formation of the space charge grating in this crystal. Therefore it is possible to assume the existence of two separate gratings in cadmium telluride for explanation of untrivial spectra of gain factor and diffraction efficiency.

References

1 M. B. Klein, Opt. Lett. **9**, 350 (1984).

2 R. B. Bylsma, P. M. Bridenbaugh, D. H. Olson, and A. M. Glass, Appl. Phys. Lett. **51**, 889 (1987).

3 USSR Invention Sertificat № 603276, Class G03H1/00, December 21, 1977, Published in Bull of Invention № 43, 250 (1978).

4 K. Tada and M. Aoki, Jpn. J. Appl. Phys. **10**, 998 (1971).

5. K. Shcherbin, A. Shumeljuk, S. Odoulov, P. Fochuk and G. Brost, SPIE Proc. 2797, 236 (1996).

6. Final Report on EOARD Special Project SPC-94-4099 (1995).

7. V. Shepelevich and E. M. Hramovich, Sov.Phys.: Optic & Spectroscopy **85**, 403 (1986).

8. S. G. Odoulov, S. S. Slussarenko, and K. V. Shcherbin, Sov. Tech. Phys. Lett. **15**, 417 (1989).

9. J. Frejlich, A. A. Kamshilin and P. M. Garcia, Opt. Lett. 17, 249 (1992).

10. J. Feinberg, D. Heimann, A. R. Tanguay, Jr. and R. W. Hellwarth, J. Appl. Phys. **51**, 1297 (1980).

11. Odoulov S., Soskin M., and Khizniak A., Optical Oscillators with Degenerate Four-Wave Mixing // Harwood Academic Publishers, London (1989).

12. N. Bloembergen, Nonlinear Optics // New York, W. A. Bengamin (1965).

13. A. Miller, D. A. B. Miller and S. D. Smith, Adv. Phys. **30**, 697 (1981).

14. H. J. Eichler, P. Gunter and D. W. Pohl, Springer Ser. Opt. Sci. **50**, 13 (1986).

15. H.Pedersen, P. Andersen, P. Petersen, P. Johansen, JOSA **B 13, 2569** (1996).

16. K. Walsh, T. J. Hall, and R. E. Burge, Opt. Lett. **12**, 1026-1028 (1987).

17. G. A. Brost, R. A. Motes, and J. T. Rotge, JOSA **B 5**, 1879 (1988).

18. S. Odoulov, K. Shcherbin, R. Litvinov, E. Shandarov and S. Shandarov, JOSA **B 13**, 2268 (1996).

19. L. Holtman, Phys. Stat. Sol. (a) **113**, K89 (1989).

20. S. I. Stepanov and M. P. Petrov, Opt. Comm. **53**, 292 (1985).

21. K. Walsh, A. K. Powell, C. Stace, and T. J. Hall, JOSA **B 7**, 288 (1990).

22. A. Shumelyuk, S. Odoulov, G. Brost, *"Nearly degenerate Two-Beam Coupling in photorefractive crystals with two types of movable species"*, manuscript is prepared for publication (see Attachment).

23. D. Z. Anderson and J. Feinberg, IEEE J. Quantum Electron. **25, 635** (1986).

List of Publications

During the period of the running Project three articles were issued:

S. Odoulov, A. Shumelyuk, G. Brost and C. Magde,

Appl.Phys. Letters, (1996)

S. Odoulov, A. Shumelyuk, U. Hellwig, R. Rupp, and G. Brost,

Japaneese J. Appl. Phys. (1996)

K.Shcherbin, A. Shumelyuk, S. Odoulov, P. Fochuk, G. Brost,

SPIE Proc. 2795, 236 (1996)

two publications appeared in Proceedings of the Topical Meeting on "Photorefractive Materials, Effects and Devices, PR'97", Chiba, Japan, June 1997:

A. Shumelyuk, S. Odoulov, G. Brost "Nearly Degenerate Two-Beam Coupling in $Sn_2P_2S_6$", WP20, pp. 137-176;

S. Odoulov, K. Shcherbin, A. Shumelyuk, V. Taranov, G. Brost, J.Norman, "Gain Spectra of Beam-Coupling in Photorefractive Semi-Insulating Semiconductors", FP01, pp.535-538.

and two articles are prepared for publication

A. Shumelyuk, S. Odoulov, G. Brost "Nearly degenerate Two-Beam Coupling in photorefractive crystals with two types of movable species",

S. Odoulov, K. Shcherbin, G. Brost, and J. Norman, "Study of photorefractive recording in semi-insulating semiconductors with nearly degenerate four wave mixing"